NUREG/CR-4209
SAND85-0679
R1 and RD
Printed July 1985

Comparison of Analytical Predictions and Experimental Results for a 1:8-Scale Steel Containment Model Pressurized to Failure

David B. Clauss

Prepared by
Sandia National Laboratories
Albuquerque, New Mexico 87185 and Livermore, California 94550
for the United States Department of Energy
under Contract DE-AC04-76DP00789

Prepared for
U. S. NUCLEAR REGULATORY COMMISSION

Available from

Superintendent of Documents
U.S. Government Printing Office
Post Office Box 37082
Washington, D.C. 20013-7982

and

National Technical Information Service
Springfield, VA 22161

NUREG/CR-4209
SAND85-0[illegible]9
R1 and RD

COMPARISON OF ANALYTICAL PREDICTIONS AND EXPERIMENTAL RESULTS FOR A 1:8-SCALE STEEL CONTAINMENT MODEL PRESSURIZED TO FAILURE

David B. Clauss

September 1985

Sandia National Laboratories
Albuquerque, NM 87185
Operated by
Sandia Corporation
for the
U.S. Department of Energy

Prepared for
Mechanical/Structural Engineering Branch
Division of Engineering Technology
Office of Nuclear Regulatory Research
US Nuclear Regulatory Commission
Washington, DC
Under Memorandum of Understanding DOE 40-550-75
NRC FIN No. A1401

ABSTRACT

Predictions for the response of a 1:8-scale model of a steel nuclear containment building to overpressurization are compared to experimental results. Finite element analyses were used to predict the model's response. Strains, displacements, and leak rate measurements were made at 21 different pressure levels. Comparisons of the pressure histories for strain and displacement at a point, and the spatial variation of strain and displacement are made. In addition, comparisons of a more global nature, such as the capacity of the model and the failure mode, are discussed. An evaluation of the predictive capabilities and the failure criteria is made in light of these comparisons.

CONTENTS

FIGURES AND TABLES

ACKNOWLEDGMENT

The test of the 1:8-scale model could not have been accomplished without the contributions of a number of individuals. Larry Koenig and Dwight Lambert deserve recognition for designing and implementing the instrumentation and data acquisition system. The test was supervised by Tom Blejwas and Dan Horschel. Paul Matson was in charge of site preparation. Walt von Riesemann, supervisor of the Containment Integrity Division, made many contributions to the success of the program.

1. EXECUTIVE SUMMARY

High pressure tests of scale models are being used to generate data that can be used to qualify methods for reliably predicting the response of LWR containment buildings during severe accidents. A 1:8-scale steel model was pressurized to failure using nitrogen gas in November 1984. Extensive finite element analyses of the model were conducted prior to the test. This report documents the comparisons between these analyses and the experimental results, and makes an assessment of analytical capabilities for predicting the response of steel containment due to static overpressurization. Also, the results of a post-test analysis, which gave additional insight into the model's failure, are discussed.

The 1:8-scale steel model was designed and fabricated for 40 psig internal pressure by Chicago Bridge and Iron Company following ASME pressure vessel code standards. The model consisted of a 3/16 inch thick cylindrical shell that was welded to a hemispherical head. The cylinder was roughly 14.5 feet in length and had a 14 foot diameter. Circumferential stiffening rings were attached to the external surface of the cylinder at 15 inch intervals. Two operable equipment hatches, two personnel lock representations, and seven pipe penetrations passed thru the cylinder. 'O' rings were used to form a seal between the equipment hatch sleeves and its covers. The cylinder was reinforced at all penetrations as required by ASME code.

Finite element methods were used to analyze the response of the model due to static overpressurization. Thin shell elements were used to represent the structure, and large displacement, finite strain, and nonlinear material behavior were taken into account. Rupture was assumed to occur if the equivalent membrane strain exceeded 15% (the material's strain at maximum load), or if the equivalent bending strain exceeded 20% at any point on the pressure boundary. Leakage past the equipment hatch seals was expected if a total mismatch of the sealing surfaces occurred.

The model was tested over a three day period from November 15-17, 1984 using nitrogen gas. Nearly 1000 channels of data, including strain, displacement, and leak rate measurements, were recorded at 21 different pressure levels up to and including 190 psig. Seven minutes after the pressure was increased to 195 psig, the model ruptured. No significant leakage was detected prior to rupture. The failure is believed to have initiated near the formed stiffener around equipment hatch 1 just below its juncture with circumferential stiffener 7. Visual observations during the test, strain gage data, the debris pattern, metallurgic investigations, and a post-test finite element analyses all support this hypothesis.

Although the mode of failure was not anticipated (leakage past the equipment hatch seals was expected to occur at 210 psig, prior to a rupture), the capacity of the model was overestimated by just 7.1%. The measured response of the model prior to

failure was very similar to expectations. After membrane yielding occurred, the strains and displacements increased rapidly throughout the model. The membrane yield pressure was overpredicted by roughly 10%. The overprediction was due to strain rate effects and the Bauschinger effect, which caused the yield stress of the cylinder material to be lower than that used in the analyses, which was determined from uniaxial tensile tests of the plate stock.

Predictions for strains and displacements were, in general, very close to the measured values. Bending strains in penetration sleeves, bending in the cylinder at its attachment to the fixturing, and strain concentrations in the cylinder due to penetrations were all accurately predicted. As expected, the response of the equipment hatch covers and the hemispherical dome was predominantly elastic. Bending in reinforcements adjacent to their intersection with penetration sleeves was overlooked in the analysis because the elements used to represent the reinforcements were too large to represent the bending response.

The experimental results confirmed that the equipment hatch sleeves deformed into an oval shape, and suggest that leakage would have occurred by 210 psig had the model not ruptured. As expected, rotations at the sealing surface were not significant, and therefore, did not cause any significant leakage.

The initial fracture was due to very localized response, which did not affect the overall containment response prior to failure. A post-test finite element analyses showed that the fracture was due to a breakdown in the membrane load-carrying action of the stiffeners, which resulted in high bending strains in the formed stiffener. A very localized strain concentration occurred in the cylinder near the juncture of the stiffeners because the stiffeners could not carry load efficiently. Simplifications made in the pre-test analyses resulted in inaccurate predictions for the response near the juncture of the stiffeners. Had a more detailed analysis (similar to the post-test analysis) been conducted prior to the experiment, the fracture of the formed stiffener and subsequent rupture could have been anticipated.

Finite element methods are the best tool currently available for conducting structural analyses of steel LWR containment buildings subject to severe accident loads. A finite element code must have the capability to characterize large displacement, large strain, and nonlinear material behavior. In addition, analyses of severe accidents must also include the effects of elevated temperature, which was not present in the steel scale models. The primary effect of temperature is to lower the yield stress and increase the ultimate stress for the type of steel used in most containments (SA 516 Gr70), which is easily accounted for with the material models in most applicable finite element codes. Accurate results depend to a large degree on an analyst's ability to identify critical areas of the containment. The scale model tests conducted at Sandia have provided invaluable insights

into where these areas are found. If finite element models are sufficiently detailed, very good predictions for the strains and displacements in a steel containment due to static overpressurization can be generated.

The performance of the containment system can be inferred from the strain and displacement predictions, i.e., the threshold environments (maximum temperature and pressure) for leakage and rupture can be determined. Leakage criteria for penetrations and seal geometries that were not tested in the steel scale models are being developed based on the results of separate effects experiments. These leakage criteria will depend on predictions of deformation, and will take into acount the effects of thermal and radiation aging, and aerosols. The rupture criterion for steel containments should be based on the uniaxial tensile strain at maximum load, which will yield a reasonable estimate of the bursting strength provided the maximum strain in the containment is accurately predicted. Once leakage criteria for all penetrations and seal geometries are proposed and verified, predictions for the performance of steel containments during severe accidents that can be used confidently in consequence analyses, such as probabilistic risk assessment, will be possible.

2. INTRODUCTION

The Containment Integrity Division at Sandia National Laboratories is testing scale models of containment buildings to determine their response to static, internal pressurization. The models are pressurized to failure using nitrogen gas. To date, four 1:32-scale steel models and a 1:8-scale steel model have been tested. The objective of the scale model tests is to generate a structural data base that can be used to qualify methods for reliably predicting the structural behavior of containments. Analyses were conducted prior to these tests to obtain unbiased predictions for the models' response, and also to help plan the conduct of the test and the type and location of instrumentation. The analyses used to predict the response of the 1:8-scale model to overpressurization are documented in [1]. The purpose of this report is to provide a comprehensive discussion and evaluation of the comparison between the analytical and experimental results for the 1:8-scale model. A more concise report on the same topic is available in [2].

The scale model tests are part of a series of NRC-funded programs that are investigating containment integrity during severe accidents [3]. The containment building is the last engineered barrier preventing the release of radioactive materials. During a severe accident, the pressure and temperature inside the containment could significantly exceed the design basis loads. The capacity of the containment building and the timing, mode, and location of a failure affect the consequences and risks associated with a severe accident. The containment is theoretically capable of withstanding pressures and temperatures beyond the design basis since the design is based on linear, elastic behavior with large factors of safety. No explicit calculations are made during the design process that account for the containment's ability to strain and deform plastically.

The scale models were designed and fabricated in a manner as representative of actual containments as possible, given the restrictions imposed by the size reduction. The features of the 1:8-scale model are more representative of actual containments than those of the 1:32-scale models. Three different configurations were tested at 1:32-scale, which allowed the effects of different features, such as ring stiffeners and simple representations of penetrations, to be measured. A complete description of the fabrication, analyses, and testing of the 1:32-scale models is available in [4].

The 1:8-scale model consisted of a 14 ft. diameter cylinder that was welded to a hemispherical dome, Figure 1. There were a number of penetrations through the cylinder including two operable equipment hatches, two personnel lock representations, two constrained pipe penetrations, and several unconstrained pipe penetrations. The constrained pipe penetrations passed through the cylinder at diametrically opposed points and were connected to each other by an integral length of pipe, whereas the other pipe penetrations were 'floating'. The overall length of the

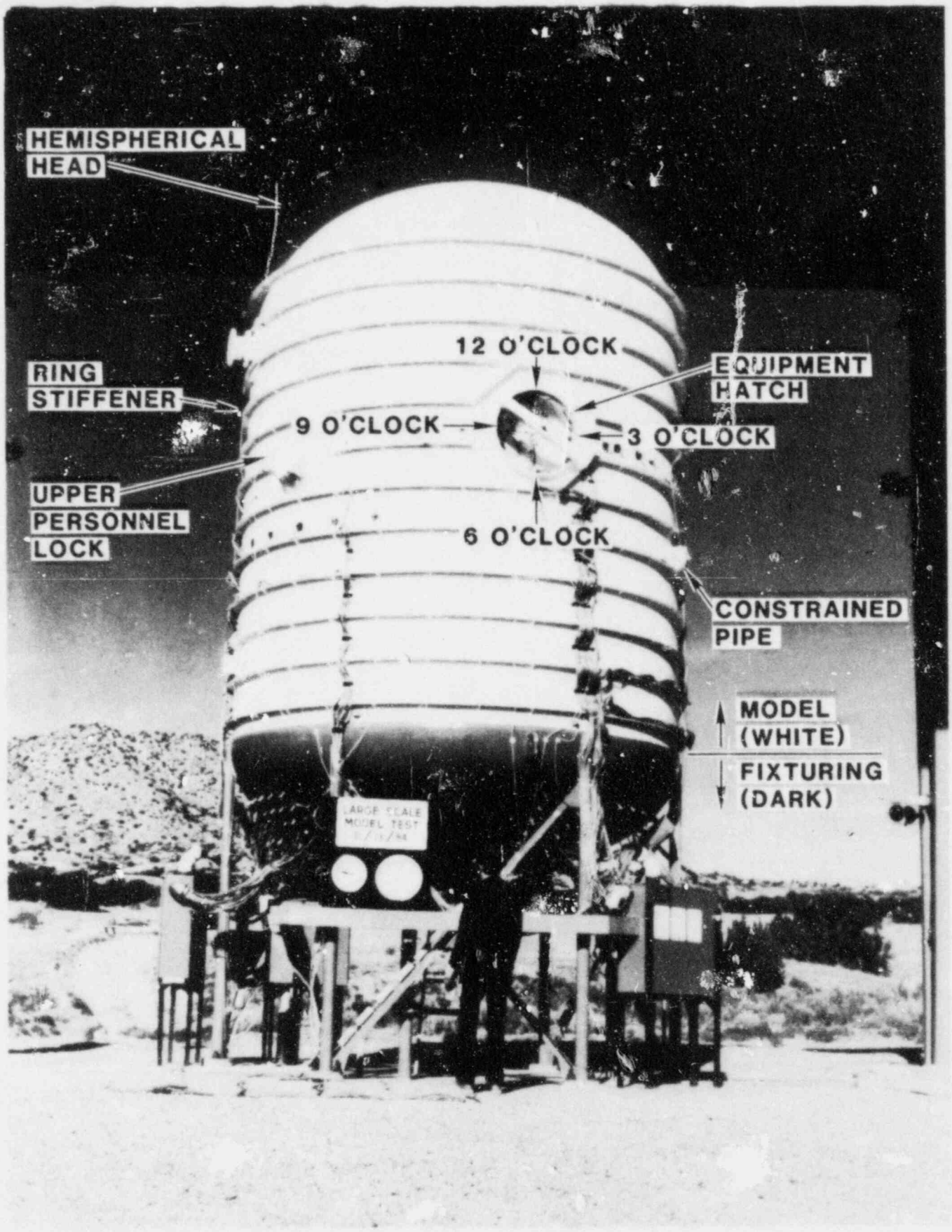

Figure 1 1:8-Scale Steel Model

cylinder was 172.5 inches. The cylinder was stiffened with 12 circumferential rings at 15 inch intervals beginning 6 inches above the lower springline. The lower springline refers to the intersection between the cylinder and the ellipsoidal base, which was considered to be part of the test fixture and was much stiffer than the model. The cylinder was fabricated from A516 Gr70 steel plate with nominal thickness of 3/16 inch. Additional details on the design and fabrication of the model are available in [5].

3 SUMMARY OF ANALYTICAL METHODS AND PROCEDURES

The predictions for the response of the 1:8-scale model to static overpressurization were based on analyses with the K.1 version of MARC, a general purpose finite element code [6]. For the most part, thin shell elements were used to represent the structure. Options that account for finite strain, large displacement, and material nonlinearities were selected. The von Mises yield criterion was used with full Newton-Raphson iteration.

Stress-strain curves for the plates used to fabricate the model were determined from uniaxial tersile tests conducted by the Process Metallurgy Division at SNLA. The test coupons were machined from remnants and cutouts for the penetrations. All of the materials tested exhibited a distinct yield plateau with significant work hardening not in evidence until strain levels of from 1.5% to 2.3% were reached. The yield stress varied from 58 ksi for the plates used to fabricate the cylinder down to 46 ksi for the constrained pipe. Elastic properties (Young's modulus, Poisson's ratio, and the shear modulus) were determined using ultrasonic techniques. Additional information on the material properties is available in [1,5]. The measured properties were input to the finite element code without significant modification. The material model did not account for strain rate effects or effects of fabrication.

A material failure (rupture) was assumed if the predicted equivalent strain exceeded 15% through the thickness (membrane), or 20% due to bending. These strain levels were based on the uniaxial tensile strain at maximum load, as well as results from the 1:32-scale models. The equipment hatch seals represented a potential leakage path that did not involve a material failure. Significant leakage past the seals was expected if the differential displacement between the sleeve and cover resulted in a loss of contact at any point between the 'O' ring seal and one of the sealing surfaces.

Five different finite element models were used to predict the behavior of various areas of the 1:8-scale model [1]. Axisymmetric models were used to predict the response of the hemispherical head, the cylinder near the lower springline, and the equipment hatch covers. It was assumed that equipment hatch covers and sleeves were structurally decoupled. The response of

the constrained pipe, the upper personnel lock (PL2), and the equipment hatches, and the response of the cylinder due to its interaction with these penetrations were predicted with three three-dimensional models, one for each type of penetration.

Strain measures calculated using MARC were converted to principal strains on the shell surfaces. The strains were then extrapolated to obtain nodal values, which could in turn be interpolated to locations corresponding to the position of instrumentation on the model. This allowed for a direct comparison of analytical and experimental results. For all plots in this report, the analytical model used to predict the response is identified using the following code: RS - axisymmetric, ring stiffened shell model, HC - axisymmetric, equipment hatch cover model, CP - 3D, constrained pipe model, EH - 3D, equipment hatch sleeve model, and PL - 3D, personnel lock 2 model. These models are described in detail in [1].

4. HIGH PRESSURE TEST

Pressure was introduced to the model over a three day period during November 15-17, 1984. Nearly 1000 channels of data, including strain, displacement and leak rate measurements, were recorded at 21 different pressure levels. For the most part, the reliability and quality of the data was exceptional. The only notable exception was the displacement data gathered using the coordinate determination system. The theodolite measurements were very noisy and inconsistent with measurements from hard wired transducers, and consequently, the displacement data obtained with the coordinate determination system was not used.

Details of the conduct of the test and test results can be found in [7,8]. Data were recorded after the model stabilized, which generally took twenty to thirty minutes from the time a pressure step was initiated. Although the pressure inside the model equilibrated very quickly after a step was initiated, the strains and displacements increased over a relatively long period of time, especially after membrane yielding of the cylinder began. Four strain channels and two displacement channels were continuously monitored, and when the rate of change in these readings was sufficiently small, the model was said to be stabilized. Pressure was held constant for the two overnight periods at 140 and 170 psig. At these pressure levels, data was recorded after the model had stabilized, and also the following morning; only the data recorded in the morning are included in this report. The model did continue to expand and strain slowly overnight [8].

The model ruptured seven minutes after the pressure was increased from 190 to 195 psig. No significant leakage was detected up to 190 psig. While the pressure was being held at 165 psig, a theodolite operator reported a crack in the formed stiffener around equipment hatch 1 (EH1) just below the weldment

attaching it to ring stiffener 7, but it was believed at that time that the crack was only in the paint. During a post-test interview, the operator stated that he had observed the crack growing at higher pressures. A strain gage adjacent to this formed stiffener was monitored during the last pressure step. Over a period of twenty seconds immediately preceding the rupture, the strain at this point jumped from 3.4% to 8.2%. The five other strain and displacement channels that were being monitored did not record unusually large increases prior to rupture. The model fragmented into at least twelve pieces, which scattered in a direction generally opposite to the original orientation of equipment hatch 1.

Based upon the location of the fragments, and the observations and data described above, the failure of the model is believed to have initiated with the observed crack in the formed stiffener near EH1. Similar cracks were found during post-test examinations at symmetrically located joints around both equipment hatches, which indicates that the failure would be repeatable given the same geometry and fabrication techniques. Metallurgic investigations indicated that ductile tearing was the failure mechanism, and there was no evidence of any material defects or loss of strength near the weldment.

5. GLOBAL RESPONSE

The overall response of the model prior to failure was similar to that obtained for the 1:32-scale models [4]. After membrane yielding of the cylinder occurred, the strain and displacements increased rapidly throughout the model. The predicted membrane yield pressure was 180 psig. Membrane yielding for most of the cylinder occurred between 155 and 171 psig, which is 14% to 5% lower than predicted. The observed membrane yield pressure differed throughout the model primarily due to variations in the thickness of the plate materials comprising the cylinder. Six thickness measurements were made on each plate before they were rolled to the cylindrical shape; the measurements ranged from 0.186 inch to 0.210 inch (at one corner of one plate, a thickness of 0.227 inch was recorded, but that was an anomaly). In the analyses, the cylinder was treated as a shell with uniform thickness (the average plate thickness, 0.197 inch, was used) and material properties, and consequently, initial membrane yielding was predicted to occur at the same pressure level throughout the cylinder. The membrane yield pressure is directly proportional to the cylinder wall thickness. Therefore, thickness variations of 0.186 inch to 0.210 inch would account for a 10.5% difference between the minimum and maximum membrane yield pressure (the effective thickness of the stiffeners is also accounted for), compared to the approximately 9% scatter that was measured. The "average" overprediction of membrane yield pressure was actually anticipated prior to the test [9]. As explained in Section 6.1, the yield stress of the cylinder material was actually about 10% lower that that measured in the uniaxial tensile tests of the plate materials due to strain rate effects and the Bauschinger

effect. This decrease in the yield stress was not accounted for in the analyses.

In general, the predictions for strain and displacement were very good. The expected locations and magnitudes of bending strains and strain concentrations compared favorably with experimental data. Reinforcements were not highly strained, except immediately adjacent to sleeve penetrations, where bending strains were measured in some cases. The dome remained essentially elastic during the course of the experiment, as expected. Table 1 compares the test and analysis results for a number of items that give an overall impression of the model's response, including the cylinder's membrane yield pressure, the location and magnitude of the maximum strain, and strain concentration factors (SCF) in the cylinder adjacent to equipment hatch 2 (EH2) and personnel lock 2 (PL2).

Table 1 Global Comparisons

	Test	Analysis
Membrane Yield Pressure	155-171 psig	180 psig
Location of Maximum Strain	EH Sleeve	EH Sleeve
Maximum Strain	5.4%	6%
SCF: EH2	1.28	1.50
SCF: PL2	1.66	1.60
Model Capacity	195 psig	210 psig
Failure Mode	Rupture	Leakage
Location of Failure	Formed Stiffener at EH1	EH Seals

The structural response parameters of most importance to risk assessment are the capacity of the containment, and the timing, mode, and location of a failure. The predictions and the experimental results for these parameters are also contrasted in Table 1. The timing of the failure is not included since the time dependence of the accident loads was not duplicated in this test. However, since the loading can be treated as quasistatic, the timing of the failure could be determined simply by identifying at what time into the accident the internal pressure exceeds the containment capacity. The measured capacity of the 1:8-scale model, 195 psig, was 7.1% less than the predicted capacity of 210 psig. However, the model ruptured catastrophically, rather than failing due to leakage from the equipment hatch seals, as expected. The locations of the expected failure and the initiation of the rupture were in the same vicinity, near equipment hatch 1. The incorrect prediction for the failure mode was disappointing, even though most other parameters of interest were predicted with reasonable accuracy.

A finite element analysis was conducted after the test with a model that characterizes the geometry of the stiffener details

around an equipment hatch more accurately than the earlier model. Details of the post-test analysis are presented in Appendix A. As shown in Figure 2, the short extension of the vertical section of the formed stiffener below circumferential stiffener 7 was not included in the pre-test finite element model. By not including this extension, equilibrium at the stiffeners juncture was satisfied with only membrane forces, and consequently the predicted strains at the juncture were similar to "free-field" strains at the same elevation. For the actual geometry, bending moments in the formed stiffener are required for equilibrium. The strength of the stiffeners is reduced when they carry the load by bending rather than membrane action. In the post-test analysis, the maximum strain was due to bending in the formed stiffener just below its juncture with stiffener 7. By 165 psig, the calculated maximum principal strain was almost 16%. (The theodolite operator first noticed the crack in the formed stiffener at 165 psig.) Furthermore, a strain concentration arose in the cylinder adjacent to the juncture of the stiffeners, where the maximum principal strain reached 11.5% at 195 psig, the pressure at which the model ruptured. This result suggests that the rupture criterion is valid, and that the mode of failure could have been anticipated if a more detailed analysis had been carried out prior to the test.

The simplification in the geometry made for the pre-test analysis was motivated by the reduction in the size and complexity of the finite element model it enabled. The justification for the change was based on (1) the short length of the extension, (2) the belief that a small amount of yielding would relieve stress concentrations at the juncture. Bending strains in other areas of the scale model did not increase rapidly until after membrane yielding of the cylinder had begun. However, the post-test analysis showed that the bending strains in the formed stiffener had increased steadily to roughly 16% by 165 psig. The distinction between the bending response at the stiffeners' juncture and the bending response at most other locations, such as the cylinder at the lower springline, is that the former was load controlled whereas the latter was displacement controlled (dictated by a mismatch in the membrane solutions for displacement at two intersecting shells). Since large displacements do not begin until after membrane yielding begins, bending strains that are displacement controlled are limited by the "free-field" strain in the cylinder. With the benefit of hindsight, areas where bending could arise should be carefully analyzed, particularly so where it involves a breakdown in the membrane action for carrying load.

The leakage criterion for the equipment hatch seals was not refuted nor wholly verified by the test. It was demonstrated that considerable relative deformation of the sealing surfaces could be tolerated without significant leakage. Neither gapping (out-of-plane separation of the sealing surfaces) or significant rotation was detected, and obviously, they did not contribute to leakage. The concept of the onset of leakage coinciding with a complete radial mismatch of the sealing surfaces (i.e., seal

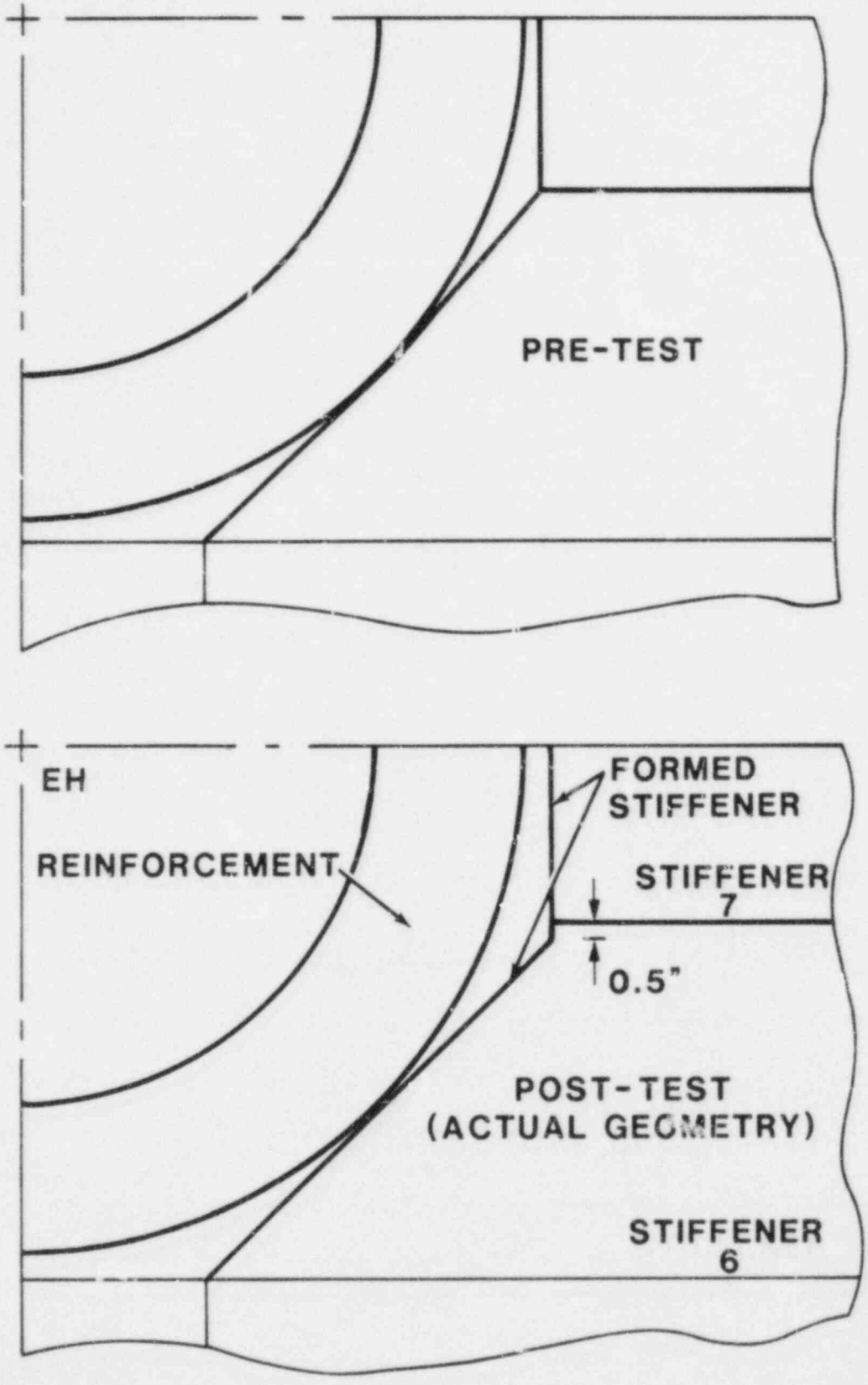

Figure 2 Geometry of Formed Stiffener Near an Equipment Hatch

material not in contact with both surfaces) still appears to be plausible. Leakage was expected to occur by 210 psig. The approximate deformed shape of the sleeve, as reconstructed from displacement measurements at 190 psig, Figure 3, suggests that leakage was imminent at the time of rupture.

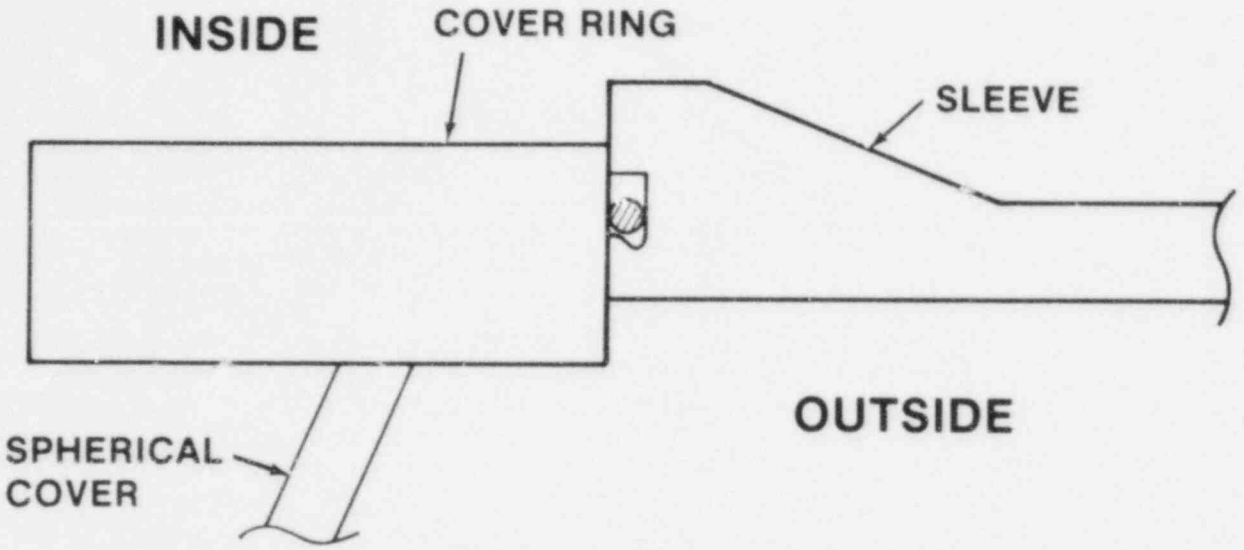

At 3 O'clock

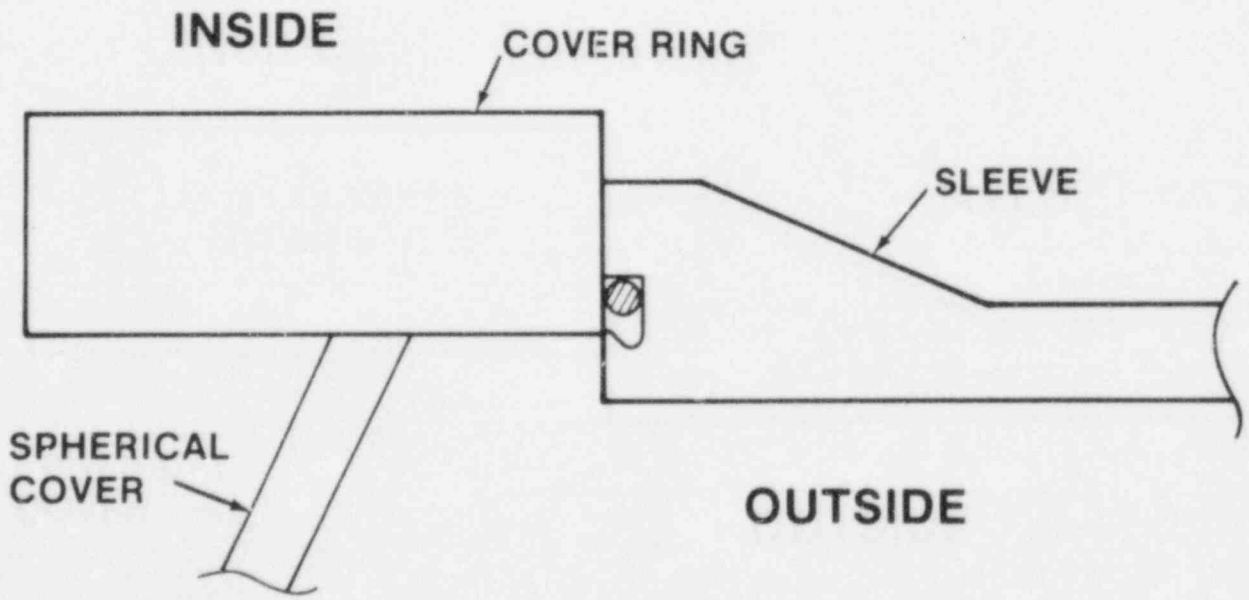

At 12 O'clock

Figure 3 Approximate Deformed Shape of EH Sleeve at 190 psig

6. CYLINDER AND DOME

The location of strain gages and displacement tranducers on the cylinder and dome are shown schematically on the developed surface (stretchout) of the model in Figure 4. Appendix B contains plots of the data and the analytical prediction versus pressure for all gages and transducers where a comparison was made, including the penetrations and reinforcements. Predictions were not made for certain areas of the model where the response was not critical. The gage numbers of instrumentation in these areas are underscored. The complete set of data is available in [10]. The exact locations of the strain gages and displacement transducers are contained in [5].

6.1 "Free-Field" Behavior

The response of the model away from the effects of penetrations is referred to as the "free-field" behavior. The "free-field" response represents an upper bound for predictions of the model's capacity, and serves as a convenient reference for evaluating the response near penetrations, for instance the magnitude of strain concentrations. Furthermore, it is the least complicated area to predict analytically. The response measured with the line of strain gages numbered 61 thru 94 at 295° on the cylinder and dome was placed in this category, since the nearest major penetrations were over 45° away. Several other strain gages were also included in this grouping, mostly because they did not naturally fall into any other. All of the gages in this group are denoted with an F appended to the gage number in Figure 4.

Radial displacements of almost two inches and strains up to three percent were developed in the "free-field", or membrane areas of the cylinder. Experimental and analytical results for the "free-field" principal strains in the cylinder at four different elevations are plotted as a function of pressure in Figures 5-8. In the elastic range, the predicted and measured values for the maximum principal strain (primarily circumferential strain) were nearly identical. For the minor principal strain (meridional strain), the agreement between the analysis and experiment is generally not quite as good, which can be attributed to simplifications made in the analyses. The ring stiffeners were modeled implicitly in the analysis used to predict the "free-field" response of the cylinder by increasing the cylinder thickness uniformly by an amount acounting for the volume of stiffener material [1]. While this approach accurately represents the circumferential stiffness of the ring stiffened cylinder, it overrepresents its meridional stiffness because the stiffeners do not help carry meridional load. Therefore, the analysis should underpredict the meridional strain in the cylinder. In addition, small differences in the initial yield surface can cause large differences in the minor component of strain. The sharp, well defined change in the slope at the yield point that was predicted analytically was not observed during the test. The overprediction of the membrane yield pressure, which

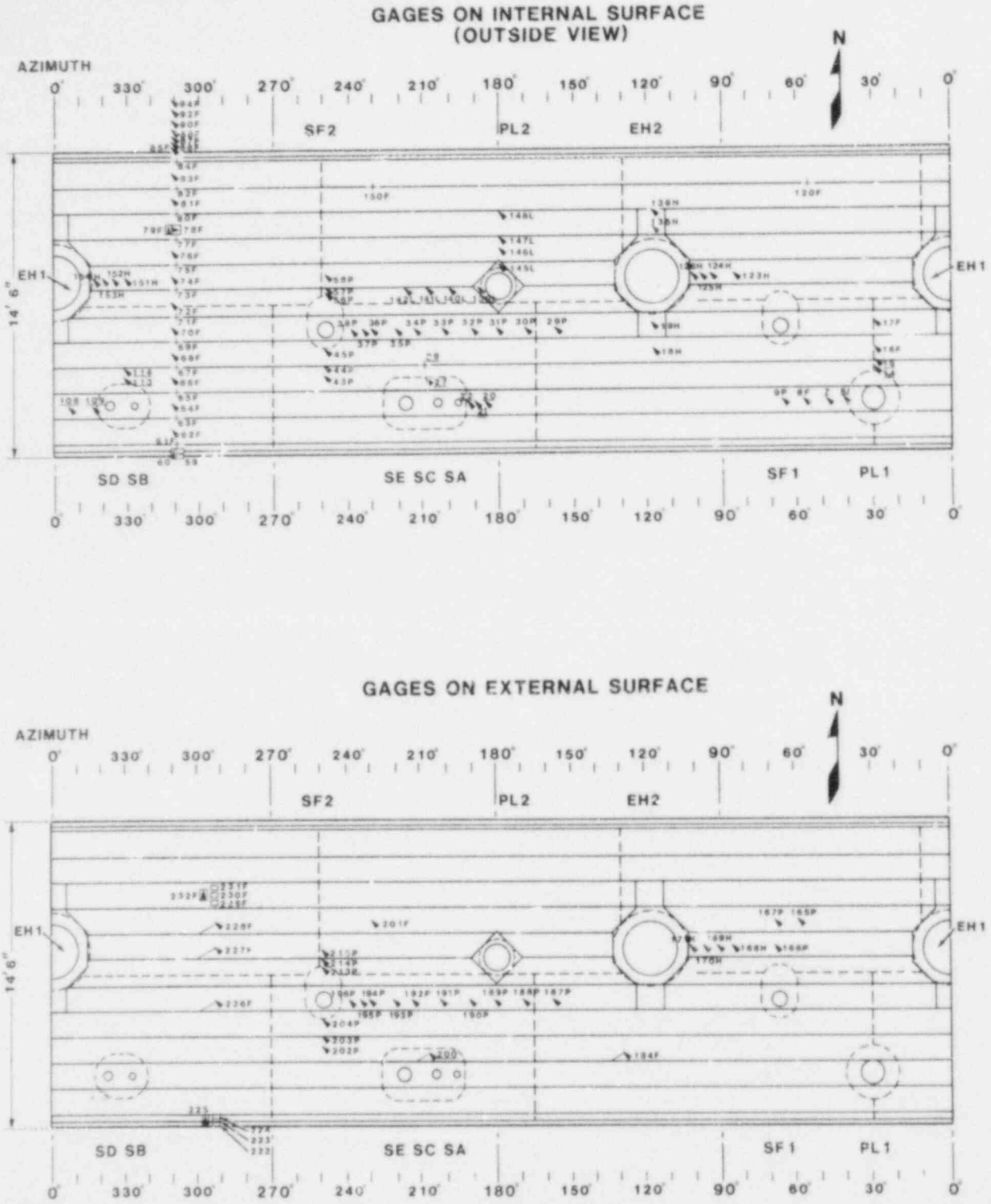

Figure 4a Schematic of Strain Gages on Cylinder and Dome

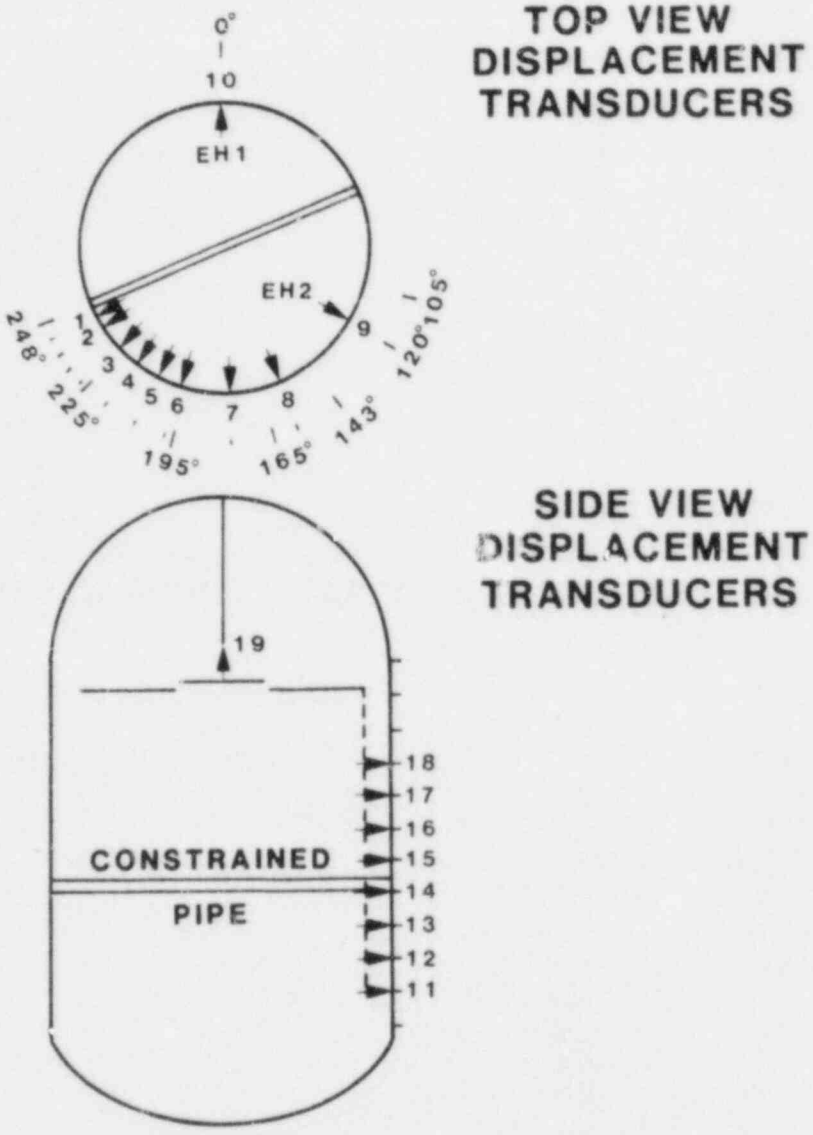

Figure 4b Schematic of Displacement Transducers on Cylinder and Dome

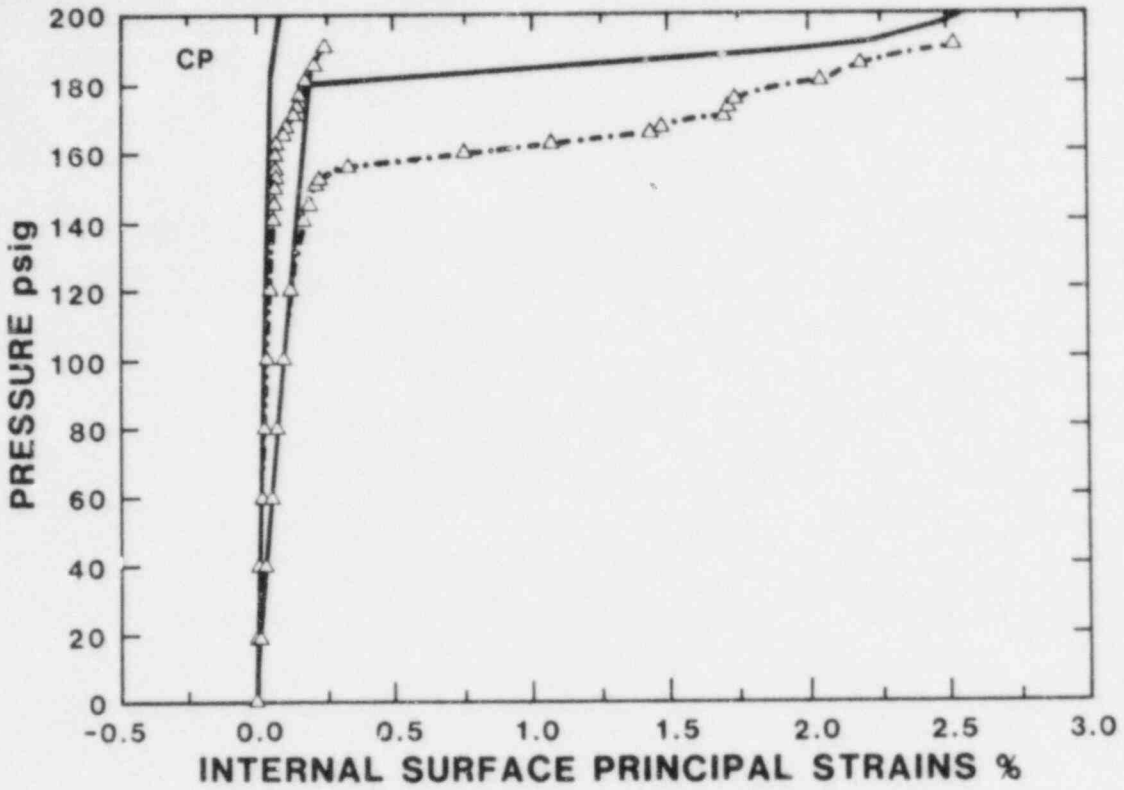

Figure 5 "Free-Field" Strains vs. Pressure (SG 66)

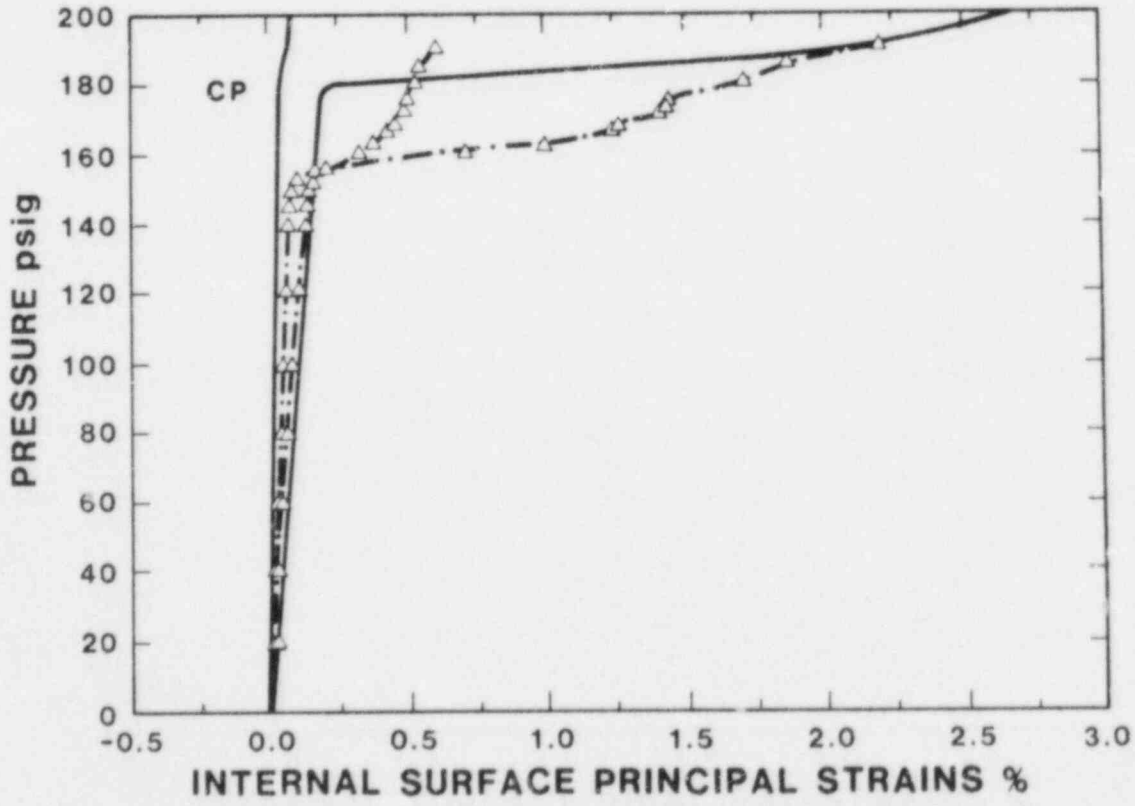

Figure 6 "Free-Field" Strains vs. Pressure (SG 67)

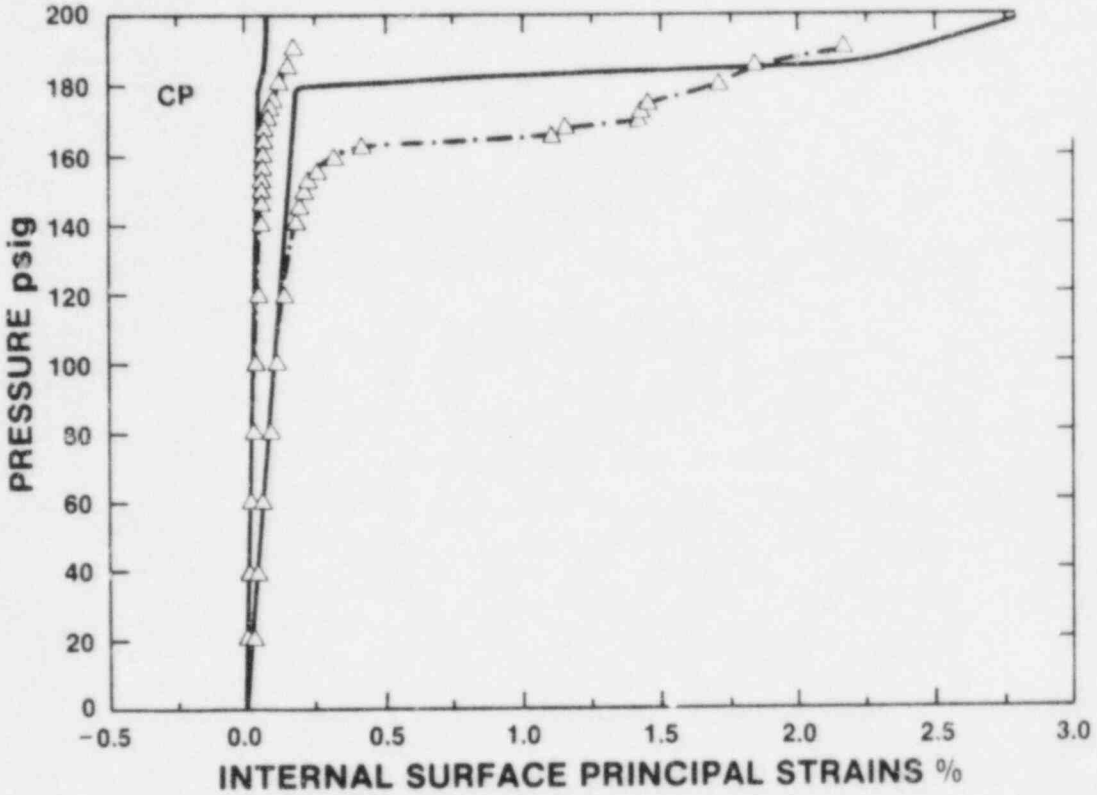

Figure 7 "Free-Field" Strains vs. Pressure (SG 74)

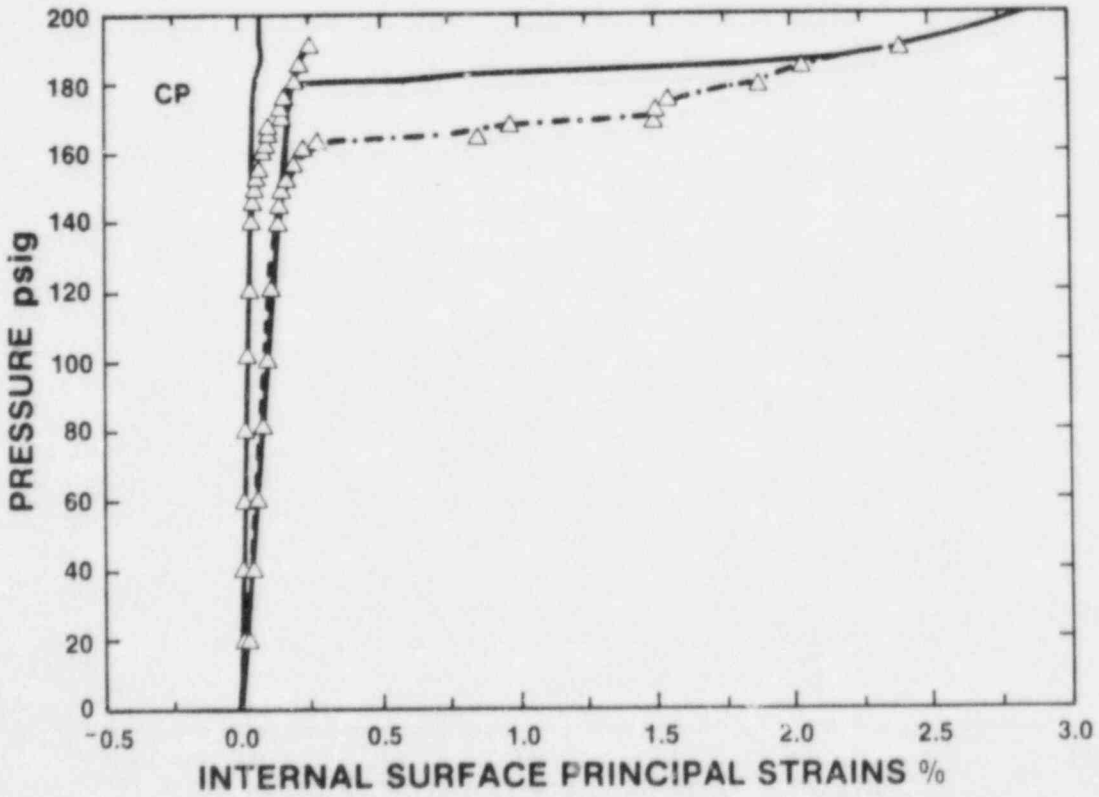

Figure 8 "Free-Field" Strains vs. Pressure (SG 75)

was first mentioned in Section 5, is clearly evident. The yield stress of the cylinder material was less than that measured for the plate materials using uniaxial tests due to strain rate effects and the Bauschinger effect. The average strain rate during the high pressure test was approximately two orders of magnitude less than that in the uniaxial tensile tests, which reduced the yield stress four to five percent. The Bauschinger effect refers to the phenomenon whereby the yield stress in tension or compression is reduced if the material has been previously yielded in the opposite sense. When the plates comprising the cylinder were rolled into the cylindrical shape, the internal surface underwent compressive yielding. Internal pressurization results in tensile yielding in the cylinder. As described in Appendix C of [5], simple calculations show that about one-quarter of the wall thickness yielded in compression when the plates were rolled to the cylindrical shape, and based on a reduction of the flow stress for one quarter of the wall to 55% of the original flow stress, the Bauschinger effect probably accounts for about a five percent reduction in the membrane yield pressure of the cylinder. Figures 5 thru 8 also suggest that the cylinder material may have begun to work harden at lower strain (approximately 1.5%) than it did in the uniaxial tensile tests.

The strains recorded with gages 61 to 84 at 150 psig, when the cylinder was approaching membrane yielding, and at 190 psig, by which point significant plastic strains had arisen, are plotted as a function of elevation and compared to the analytical result in Figure 9. There are two striking features of this plot: (1) the nonuniformity of the data, and (2) the change in the strain magnitudes from the bottom to the top plate, which is most evident at 190 psig,. This indicates that variations in material properties and variations in thickness in the plates used to fabricate the cylinder are partly responsible for differences between the analytical and experimental results.

Pre-test analyses indicated that the "free-field" strains in the circumferential ring stiffeners were slightly less than in the cylinder at the same elevation. Figure 10 shows that the agreement between the analytical and experimental result for the "free-field" principal strains in the circumferential ring stiffeners is consistent with the agreement obtained for the strains in the cylinder. In the rings, the minor component of strain is associated with radial strain, which is compressive since the inside edge of the rings are pushed outward while the outside edge is a free boundary. It would appear that the circumferential stiffeners behaved essentially as predicted away from penetrations. Also, strains recorded with strip gages 78 and 79 confirmed that the stiffeners do not cause high bending strains in the cylinder. The circumferential stiffeners act to increase the membrane yield pressure of the cylinder, and probably the "free-field" strength as well. However, the design of stiffeners around the equipment hatches was such that the stiffeners did not carry load in the most efficient manner, and the multiple, intersecting welds resulted in highly constrained areas that caused

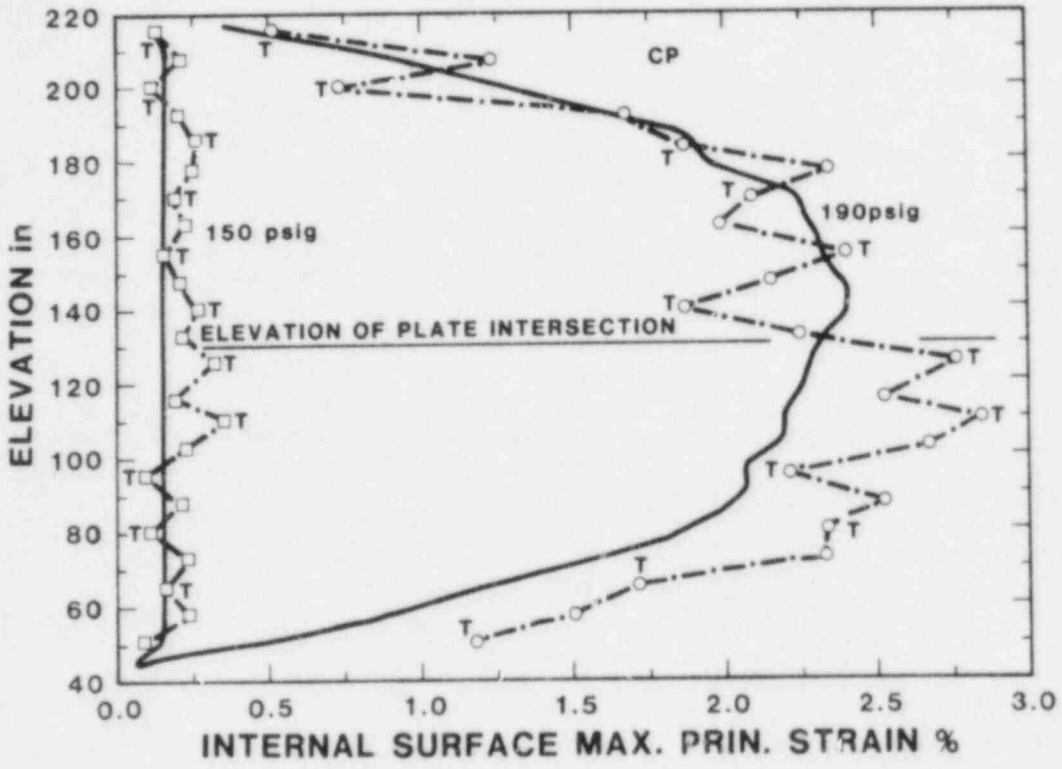

Figure 9 Variation in "Free-Field" Strain with Elevation

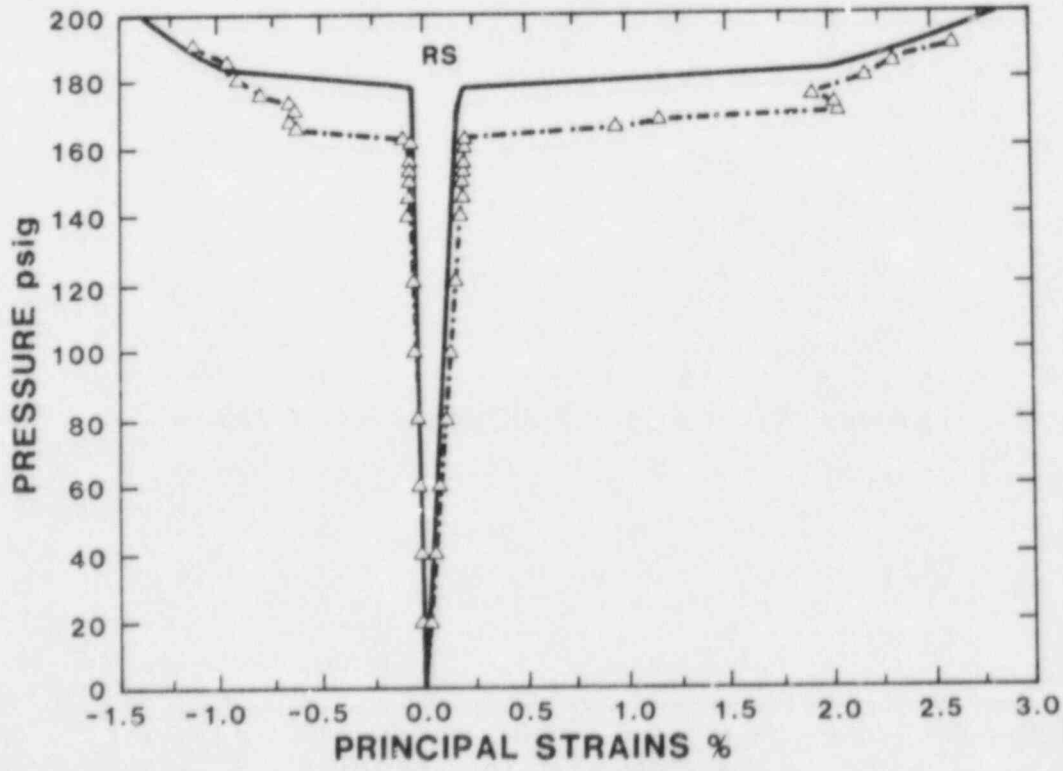

Figure 10 Free Field Strain on Stiffener 7 vs. Pressure (SG 227)

the containment strength to be less than its "free-field" strength.

Most of the dome remained elastic up through 190 psig, except for a small area near the apex of the dome. Figure 11 shows the principal strains recorded at three elevations on the dome and the predicted values vs. pressure. Analytically, the strains are uniform throughout a hemisphere subject to internal pressurization, except near the upper springline, where localized bending occurs. Although, as expected, the strains in the dome were much less than those in the cylinder, there was considerable variation in the strains recorded on the dome. This may be due to: (1) anisotropy and residual strains, which are introduced during the process of forming a doubly-curved shell, (2) thickness variations in the plates used to fabricate the dome, or (3) imperfections in the hemispherical shape.

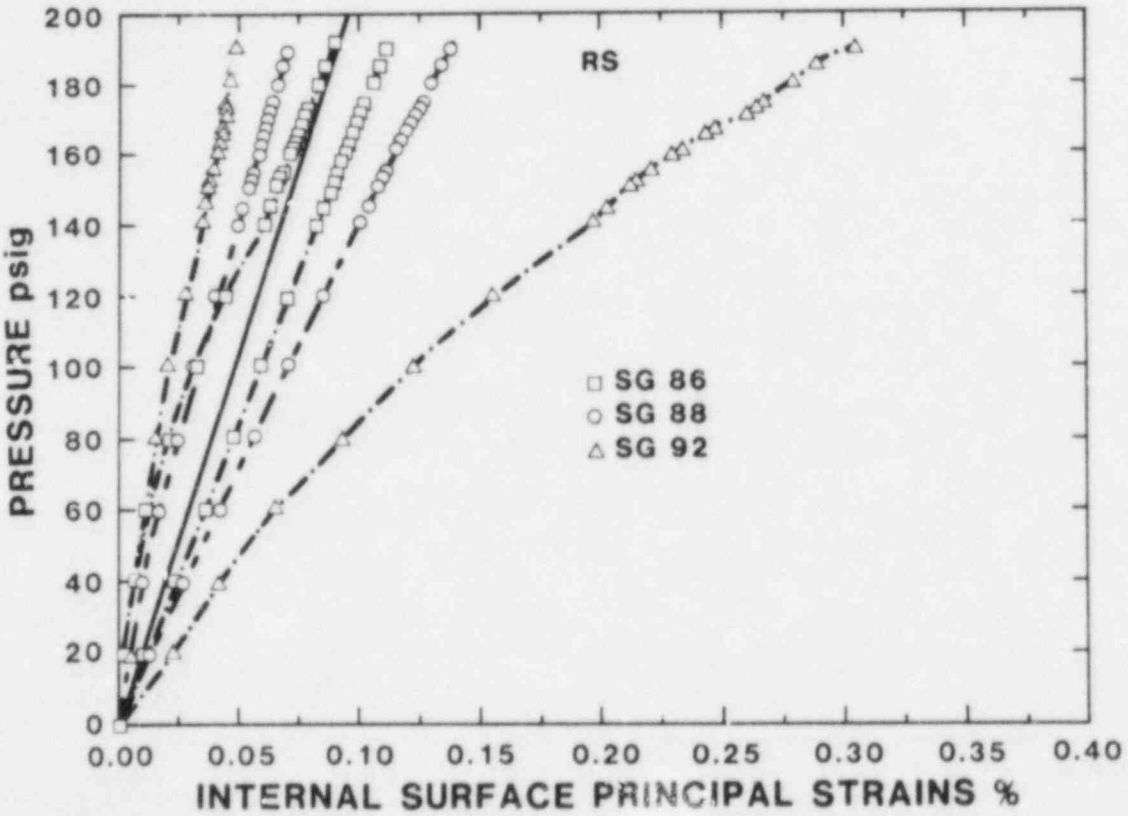

Figure 11 Principal Strains on the Dome

6.2 Effect of Constrained Pipe

The constrained pipe had a dramatic effect on the deformation of the cylinder, however, it had little or no effect on the capacity of the containment model. Gages used to measure the effect of the constrained pipe are denoted by a P following the gage number in Figure 4. Analytical predictions indicated that radial expansion of the cylinder would be essentially zero at the two locations where the constrained pipe passed thru the containment wall. The radial expansion of the cylinder increased with

distance from these penetrations, approaching the expansion of a ring stiffened cylinder without penetrations. The analytical and experimental result for the variation in displacement around the model at the elevation of the pipe's horizontal centerline is shown in Figure 12. The trends were correctly predicted, however, at 190 psig the measured displacements are less than those that were predicted. There is no obvious explanation for the overprediction of displacements, especially because the strains are generally larger than predicted at 190 psig due to the overprediction of the cylinder's membrane yield pressure. The effect of the constrained pipe on the strains in the cylinder

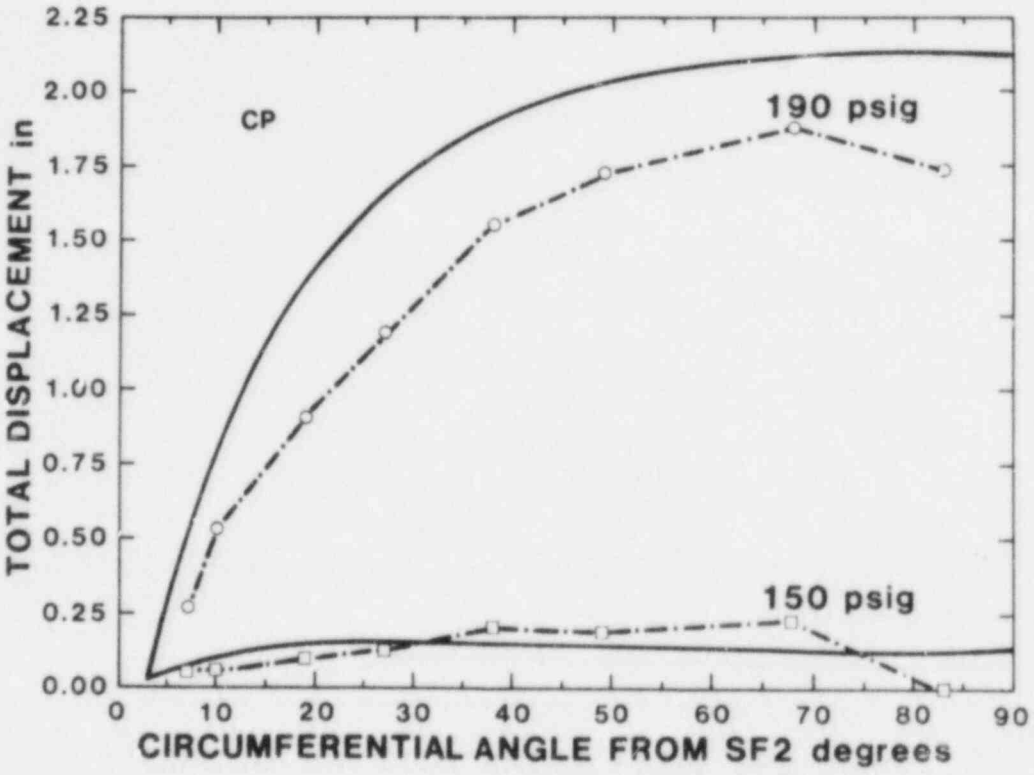

Figure 12 Variation in Displacement Away from Constrained Pipe

was very benign. Analyses suggested that the effect of the constraint is actually to reduce the strain at most points in the model. The constrained pipe was not expected to interact with other penetrations. The data appear to confirm this, because the measured response of both equipment hatches, which are not equally proximate to the locations where the constrained pipe intersects the containment wall, was very similar. The constrained pipe was not responsible for any decrease in the capacity of the containment model.

6.3 Response Near Upper Personnel Lock and Equipment Hatches

The predicted response of the cylinder in the vicinity of penetrations was characterized by an area of low strain immediately below and above the reinforcement, and an area of high

strains adjacent to the reinforcement at the elevation of the penetrations' centerline. Qualitatively, the test confirmed this behavior. At 190 psig, the maximum principal strain recorded above and below the upper personnel lock and equipment hatch 2 were approximately 1.25%, compared to about 2.25% for the "free-field" strain at the cylinder's midheight. In the cylinder adjacent to the reinforcement at the elevation of the penetrations' centerline, the maximum principal strain was as high as 3.65% at 190 psig. These strain concentrations reduce the strength of the containment model compared to the "free-field" strength. The 1:32-scale model SC3 failed at a lower pressure than the clean shell models (SC0, SC1) due to strain concentrations around the penetration representations [4].

The strain concentrations arise due to the stiffness discontinuity between the cylinder and the penetration/reinforcement assembly. As the cylinder expands, it stretches in the circumferential direction. Because the reinforcement is thicker and therefore stiffer than the cylinder, it does not stretch as readily as the cylinder. Consequently, the cylinder must undergo additional stretching near the penetrations to accomodate radial expansion, which leads to high local strains. The severity of the strain concentration depends on the size of the opening and the combined stiffness of the penetration sleeve and the reinforcement. The strain concentration becomes more severe as the size of the opening and the stiffness of the sleeve/reinforcement increase. In the case of the equipment hatches, the opening is large, but the sleeve is not very stiff since the lack of end restraint allows the sleeve to ovalize. On the other hand, the upper personnel lock sleeve is restrained at both ends with flat covers, and so it deforms in a relatively stiff mode. Analytically, the strain concentrations for these two penetrations were of approximately the same severity, with that near the personnel lock more severe at pressures below about 210 psig, and that near the equipment hatch larger above 210 psig.

The analytical and experimental results for the strain concentration near the upper personnel lock are compared in Figures 13 and 14. Although the number of data points are small, the variation in the maximum principal strain in the reinforcement and the cylinder at the elevation of the upper personnel lock was very similar to the analytical result, as shown in Figure 13. The data suggests that the area of increased strains in the cylinder was less localized than predicted, but there are not enough measurement points to draw a firm conclusion. Figure 14 shows the principal strains in the cylinder immediately adjacent to the reinforcement as a function of pressure. Yielding was observed on the internal surface at a much lower pressure than predicted, and a distinct yield plateau was not observed. These discrepancies could be explained by changes in the material properties of the cylinder near penetrations, which were affected by fabrication procedures to a greater extent than in other areas. Specifically, additional cold working of the material probably occurred when the penetrations were installed, and the

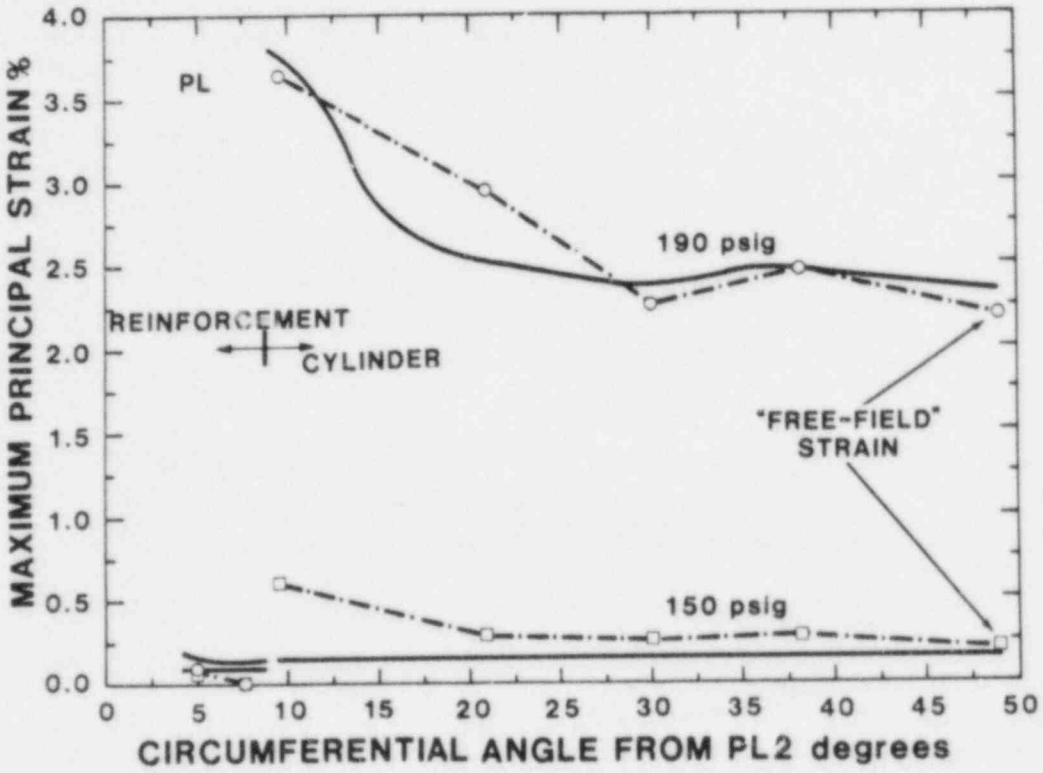

Figure 13 Variation of Circumferential Strain Away from Upper Personnel Lock

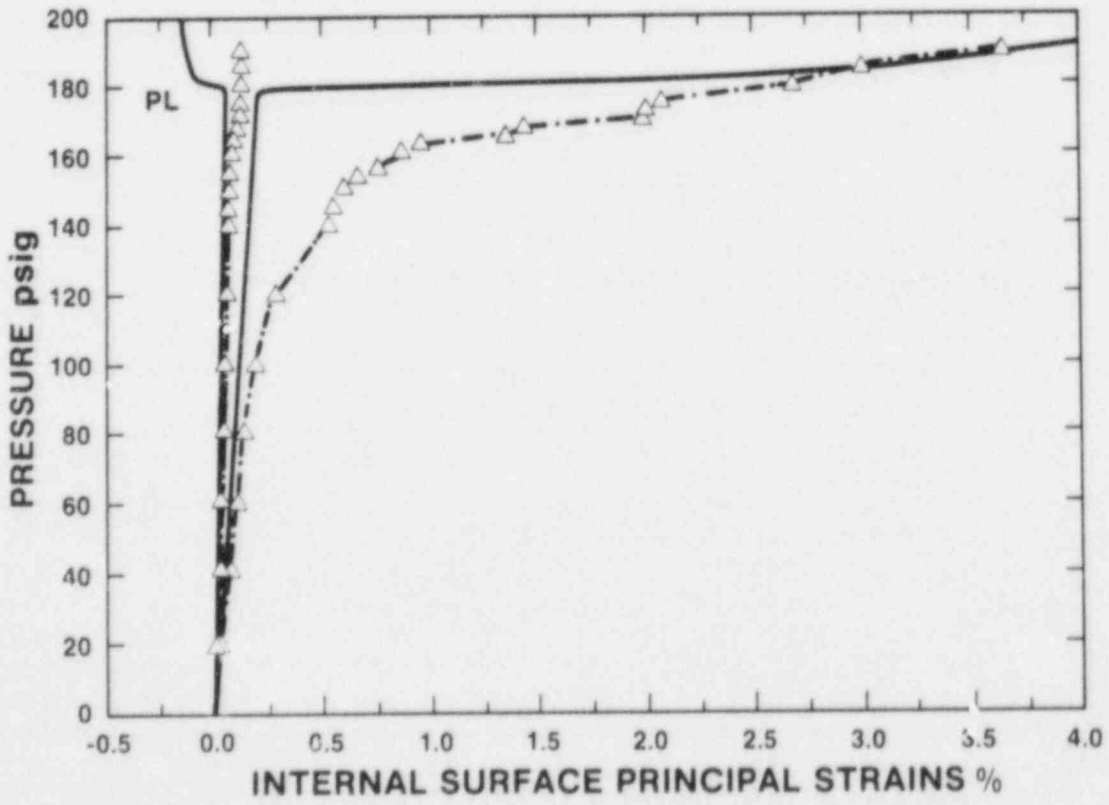

Figure 14 Principal Strains at SG 139 vs. Pressure

large amount of welding and subsequent shrinkage near penetrations may have generated significant residual stress and strain.

The variation in the measured strains near the equipment hatches, Figure 15, did not agree with the predicted behavior nearly as well as that near the upper personnel lock. The strain concentration near the equipment hatches was not as severe as expected. There was a great deal of anomalous behavior near the equipment hatches. The outward expansion of the equipment hatches was much greater than expected, about 2.25 inches at 190

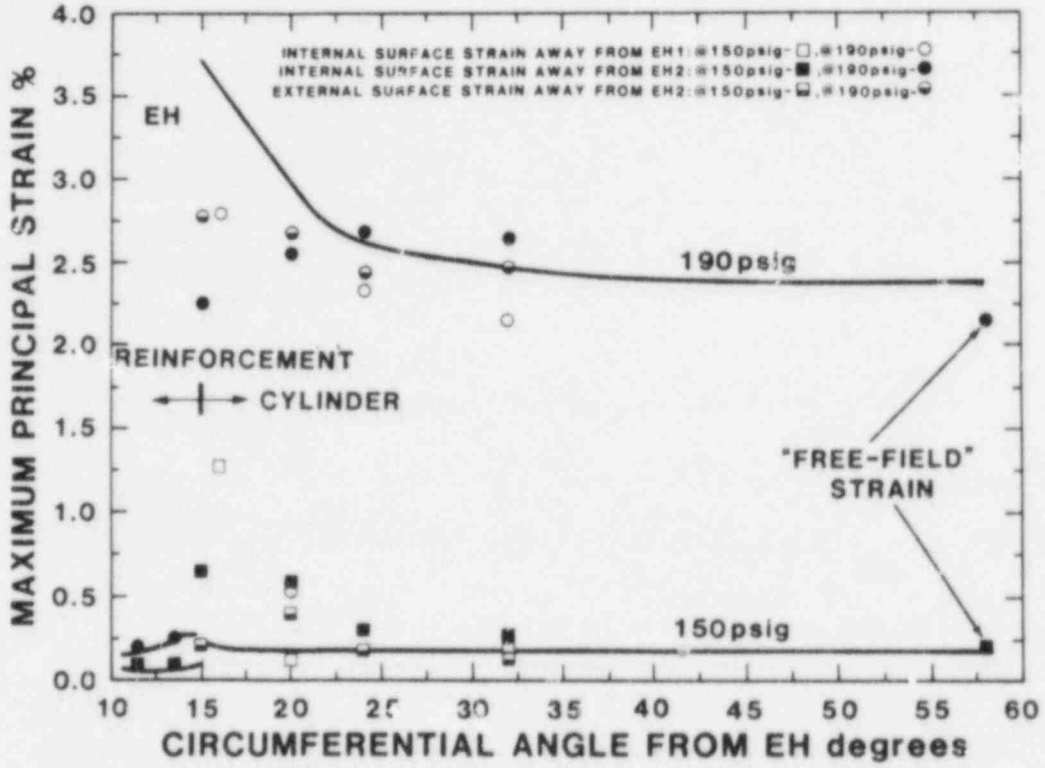

Figure 15 Variation of Circumferential Strain Away from Equipment Hatches

psig compared to an expected displacement of 1.75". Cracks were observed in the formed stiffeners around both equipment hatches, with one near equipment hatch 1 ultimately leading to the rupture of the model. As shown in Figures 16 and 17, Gage 154 shows a great deal of yielding at low pressure, while Gage 153 registered exceptionally stiff behavior. Despite the increased sophistication of the model used for the post-test analyses, there was very little change in the strains calculated at these gages. Thickness variations and local changes in the material response due to fabrication effects are one possible explanation for the discrepancies between the analytical and experimental results at Gages 153 and 154.

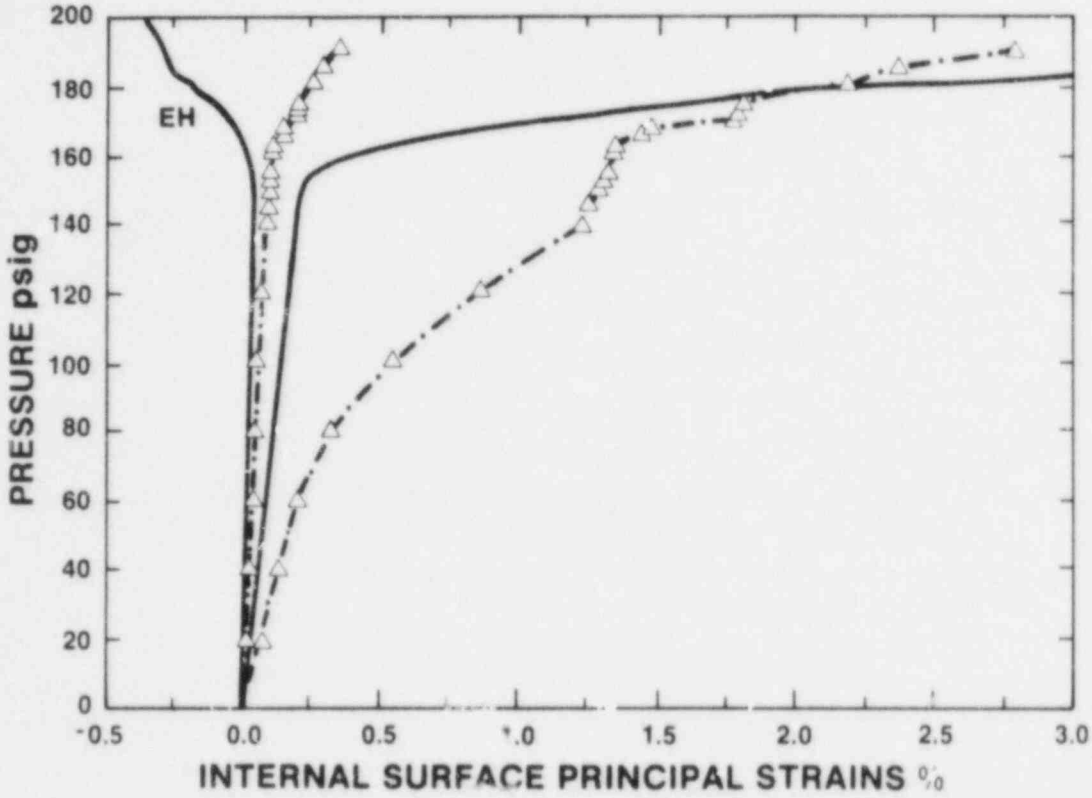

Figure 16 Principal Strains at SG 154 vs. Pressure

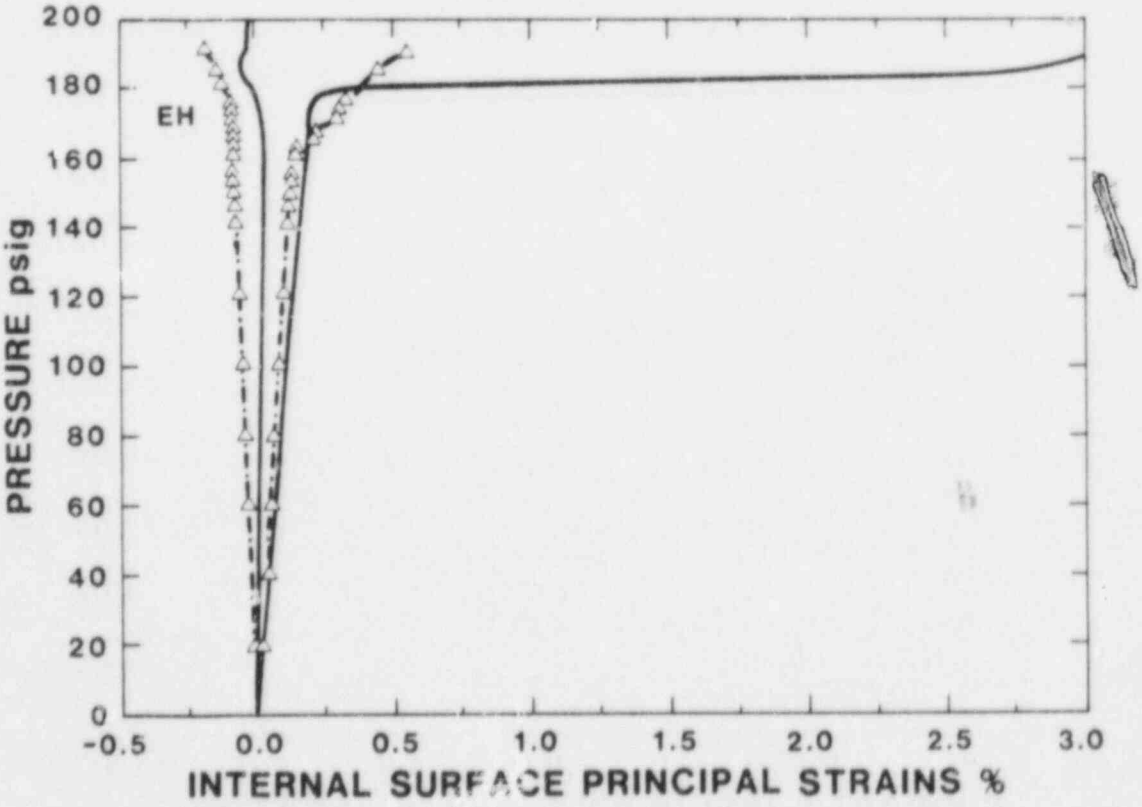

Figure 17 Principal Strains at SG 153 vs. Pressure

Several months after the test, it came to light that analyses and experiments conducted by IITRI some 20 to 25 years ago arrived at the same conclusion, that is, reinforcements in a plate (or shell) cause strain concentrations that reduce the structure's pressure capacity [11]. Experiments conducted by IITRI on flat plates with various reinforcement area ratios demonstrated that, as the reinforcement becomes stiffer, the pressure capacity decreases. Failure occurred in the plate material adjacent to the reinforcement by circumferential cracking. IITRI's experimental work and conclusion, while based on much simpler geometries, are consistent with the results of the scale steel models.

6.4 Bending Strains at Lower Springline

Strip gages were used to measure the bending strains at the lower springline. The response in this area was complicated by the weldment between the cylinder and base, and the misalignment between the cylinder and base that occurred during fabrication [5], which were not accounted for in the analysis. Also, the internal structure, which tends to resist rotation of the base and thereby increase the moment and bending strains in the cylinder, was not modeled. (The internal structure was a three level frame structure used to instrument the model [5].)

The meridional strains on the internal surface that were recorded with strip gage 59 are compared to the predicted range of meridional strain in Figure 18. The lower yield pressure was

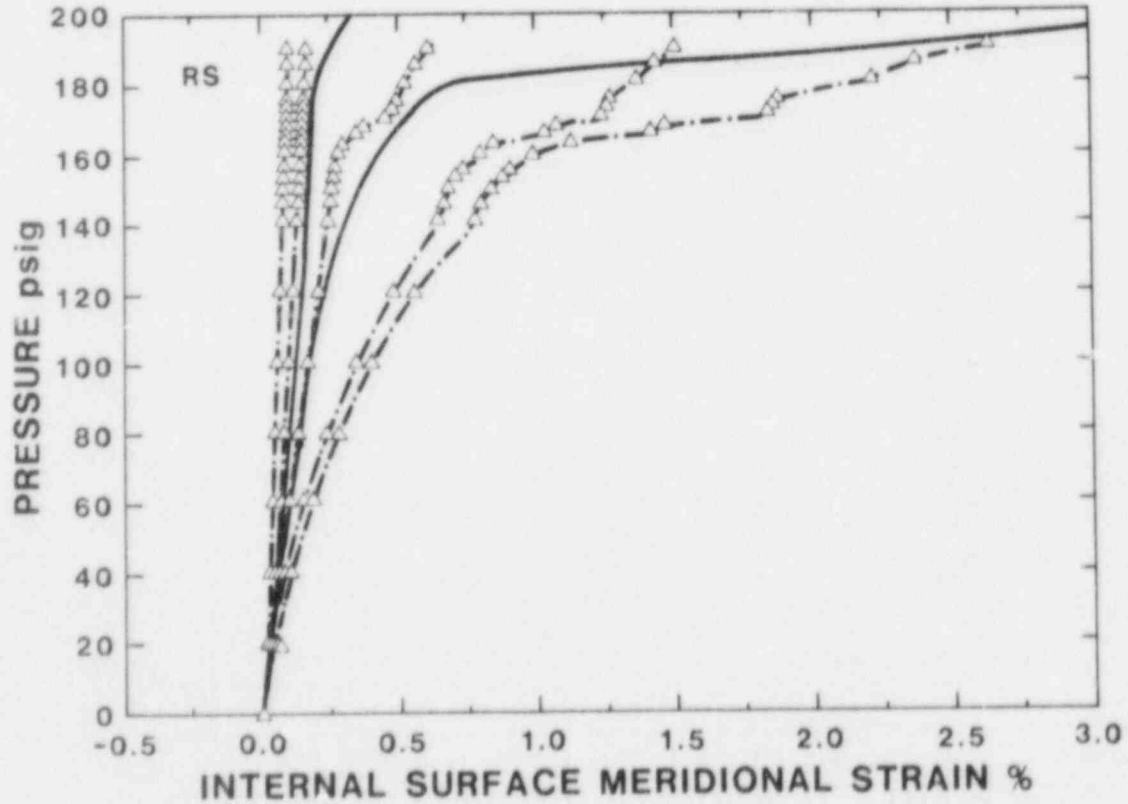

Figure 18 Bending Strains at Lower Springline

probably due to residual stresses associated with shrinkage due to welding. The distance over which large bending strains occurred, while still relatively small, was much greater than expected. Despite these differences, the magnitude of the maximum bending strain was predicted with reasonable accuracy, which is good for such a complex area (the bending response is very sensitive to the fabrication details). On the external surface, the strains were much smaller than those on the internal surface, as expected, because the bending moment is compressive on the external surface, and is therefore counteracted by membrane forces.

7. EQUIPMENT HATCHES

The instrumentation on each equipment hatch is shown in Figure 19. The equipment hatches were heavily instrumented because it was believed that they were the most likely area for a failure to occur. Strip gages were used to record the strain gradient due to bending near the sleeve-shell intersection. Unfortunately, a number of the individual elements on these gages were damaged, and the optimal measurement locations were not always available as a consequence. Additional rosettes were located on the cover and sleeve. The displacement transducers numbered 20 through 27 on equipment hatch 1, and 34 through 41 on equipment hatch 2 sensed motion parallel to the sleeve axis, and were used to calculate rotation of the sleeve near the seal. The other displacement transducers detected motion perpendicular to the surface of the sleeve or the cover tensioning ring.

The response of an equipment hatch sleeve is dictated largely by its interaction with the cylinder and reinforcement. The cover, because of its method of attachment (swing bolts around the periphery of the hatch are more typical of actual containments), was overly stiff compared to other components of the model.

7.1 Sleeve Deformation

The equipment hatch sleeves deformed into an oval shape as predicted, with the major axis parallel to the horizontal axis. Furthermore, the test confirmed that sleeve rotation near the sealing surface was small up to 190 psig. The maximum rotations occurred at 6 and 12 o'clock (roughly 2°), while somewhat smaller rotations were encountered at 3 and 9 o'clock (a maximum of 0.5°).

The change in the horizontal and vertical sleeve diameters about 1.5 inches from the seal are shown in Figures 20 and 21, respectively. The measured change in diameter of the sleeve was determined by summing the change in diameter of the cover tensioning ring and the change in radii of the sleeve relative to the cover. The changes in the sleeve diameter were generally less than predicted, which can be attributed to two modelling assumptions. The hatch cover and sleeve were assumed to be

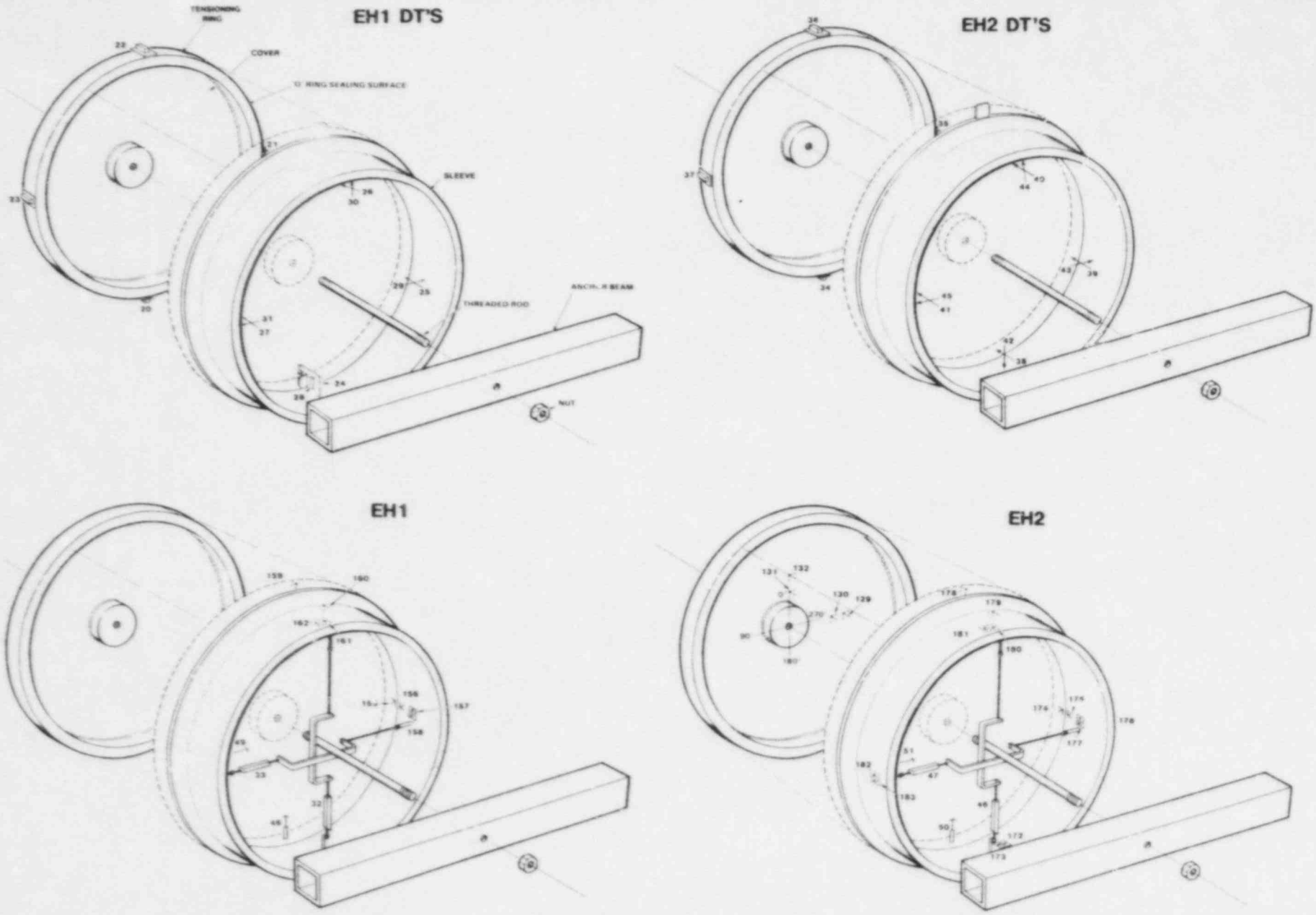

Figure 19 Schematic of Instrumentation on Equipment Hatches

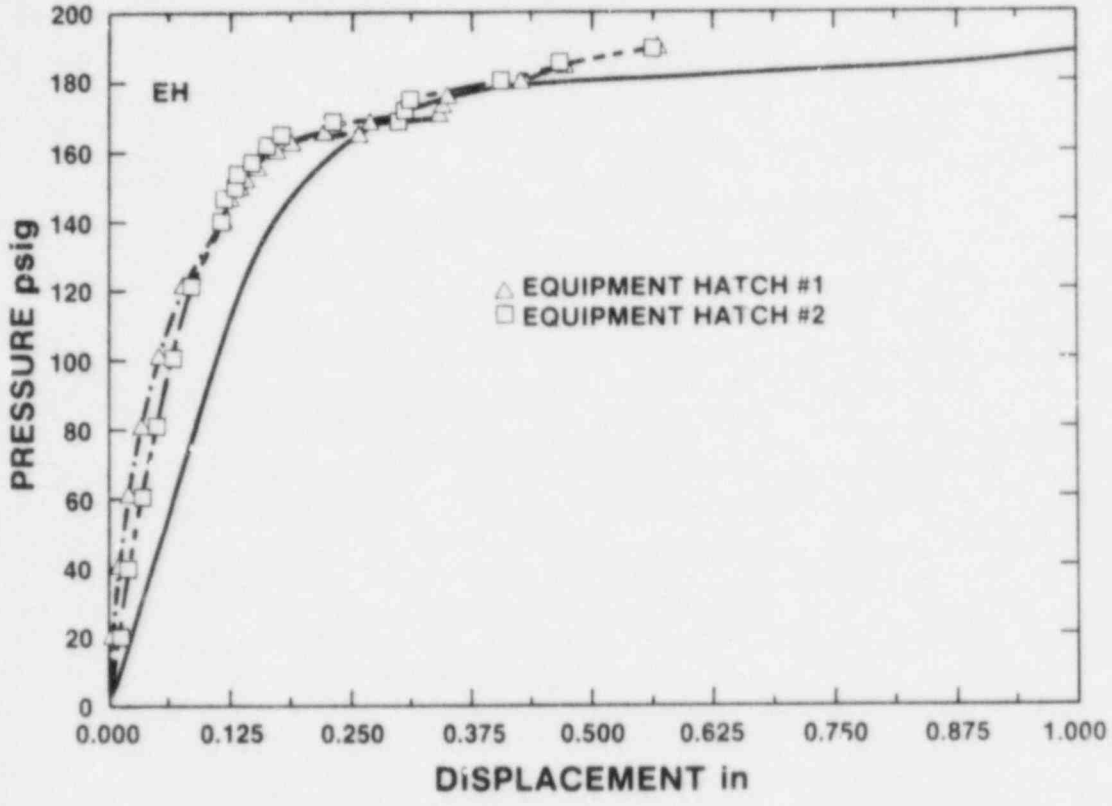

Figure 20 Change in Horizontal EH Sleeve Diameter Near Sealing Surface vs. Pressure

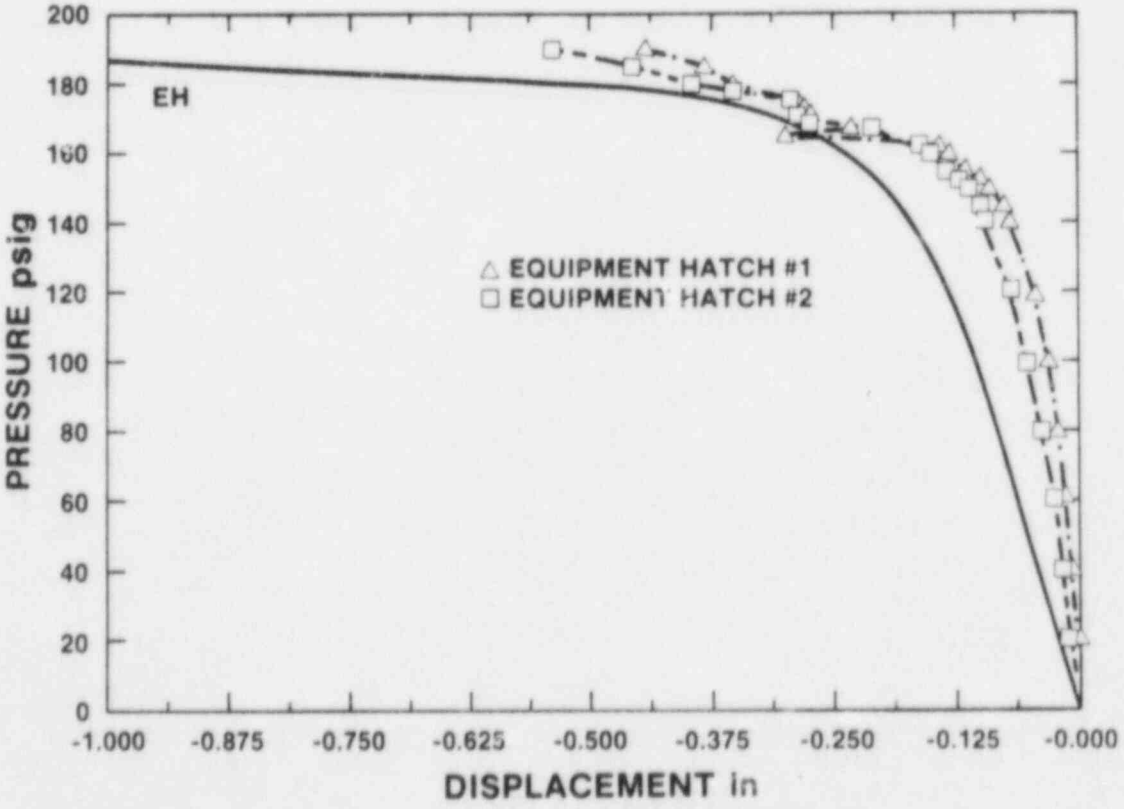

Figure 21 Change in Vertical EH Sleeve Diameter Near Sealing Surface vs. Pressure

structurally uncoupled in the analysis. The measured changes in the diameter of the cover tensioning rings suggest that friction did provide some coupling. The edge restraint on the sleeve that results from coupling would tend to prevent the sleeve from ovalizing. A second, though less important, factor contributing to the overprediction of sleeve deformation is that thin shell elements were used to model the entire sleeve. The equipment hatch sleeve tapered to a relatively thick section ($r/t \approx 13$) near the seal surface, and thin shell elements probably underestimate the stiffness of the thick section of the sleeve, resulting in an overprediction of sleeve deformation. As shown in Figure 22, much better predictions were made for the change in the diameter of the sleeve near its intersection with the cylinder, where the effects of coupling between the sleeve and cover are less pronounced, and thin shell elements are a more appropriate representation of the sleeve. The discrepancy between the analytical and experimental results noted in Figures 20 and 21 is not important enough to warrant the large increase in the cost and sophistication of the analytical model (for example, friction gap elements could be used to model the coupling of the sleeve and cover, and continuum elements to model the thick section of the sleeve) that would be required to improve the accuracy.

The experimental results verify that the sleeve deformation is dictated by the deformation of the containment wall. The sleeve diameter from 3 to 9 o'clock increased at its intersection

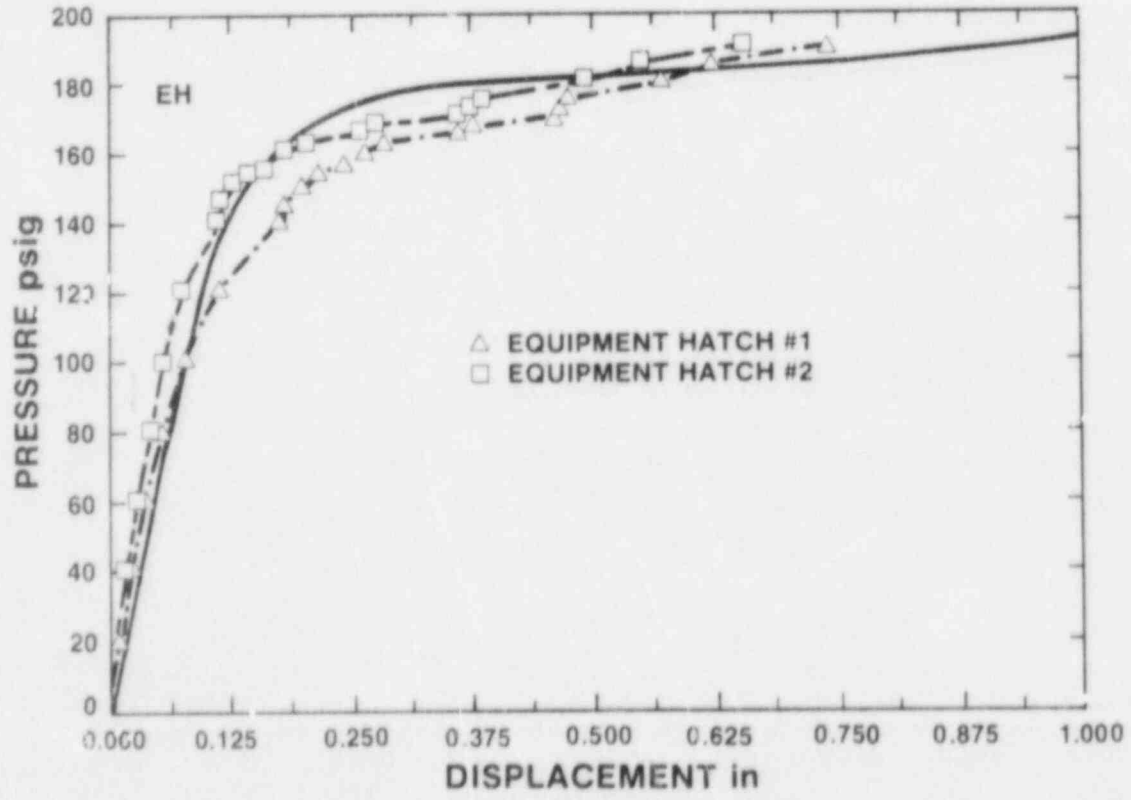

Figure 22 Change in Horizontal EH Sleeve Diameter Near Its Intersection with Reinforcement vs. Pressure

with the reinforcement to accomodate radial expansion of the containment wall. The change in diameter is approximately $\pi\varepsilon d$, where ε is the average strain in the cylinder at the elevation of the hatch, and d is the diameter of the sleeve. At 190 psig, the "free-field" strain at the elevation of the equipment hatches was 2.35%, which, by this theory, should result in a 0.675" increase in the diameter from 3 to 9 o'clock. As can be seen in Figure 22, this was very close to the experimental result. Because the ends of the equipment hatch sleeve were unrestrained (friction coupling of the cover and sleeve actually did provide some restraint, but it is neglected for purposes of this discussion), it is possible for the sleeve to deform into an oval shape. This mode of deformation is not very stiff since it does not cause stretching of the sleeve midsurface. However, the containment wall does not stretch in the meridional direction, and consequently it resists a decrease in the vertical diameter of the sleeve at their intersection. The restraint to ovalization due to the containment wall contributes to the high strains at 6 and 12 o'clock near the sleeve's intersection with the reinforcement.

7.2 Bending Strains in Sleeve

Initial yielding and the highest strains in the model were detected in the equipment hatch sleeves at 6 and 12 o'clock near the intersection with the cylinder, as predicted. The large bending strains at these locations are a direct consequence of the deformation mechanics, as explained above. The meridional strains measured at 6 and 12 o'clock are plotted in Figure 23 along with the analytical result at 150 psig and 190 psig. The comparison is favorable, except in the immediate vicinity of the intersection between the sleeve and reinforcement. In the analysis, the intersection is modeled as if the connection between the reinforcement and sleeve occurred along a line, when in fact it occurs over a finite width. This neglects the shear stiffness of the reinforcement. Consequently, the bending strains along a distance corresponding to the thickness of the reinforcement and weldment are, not surprisingly, lower than predicted. For points more than two inches from the intersection, the strains were very small, despite the large deformations of the sleeve due to ovalization. Figures 24 and 25 show the meridional and circumferential strains on the sleeve of equipment hatch 1 at 12 o'clock approximately 1.4 inches, and 0.6 inches inward from the intersection. The circumferential component of strain is also large near the sleeve's intersection with the reinforcement; because the containment wall resists a decrease in the vertical diameter at this location, some stretching must occur. The Bauschinger effect should be less apparent on the concave surface of the sleeve because the rolling process caused compressive yielding on that surface, and the meridional strain due to internal pressurization was also compressive. The accuracy of the predictions for the strains in the sleeve is very good, given the complicated geometry of the area.

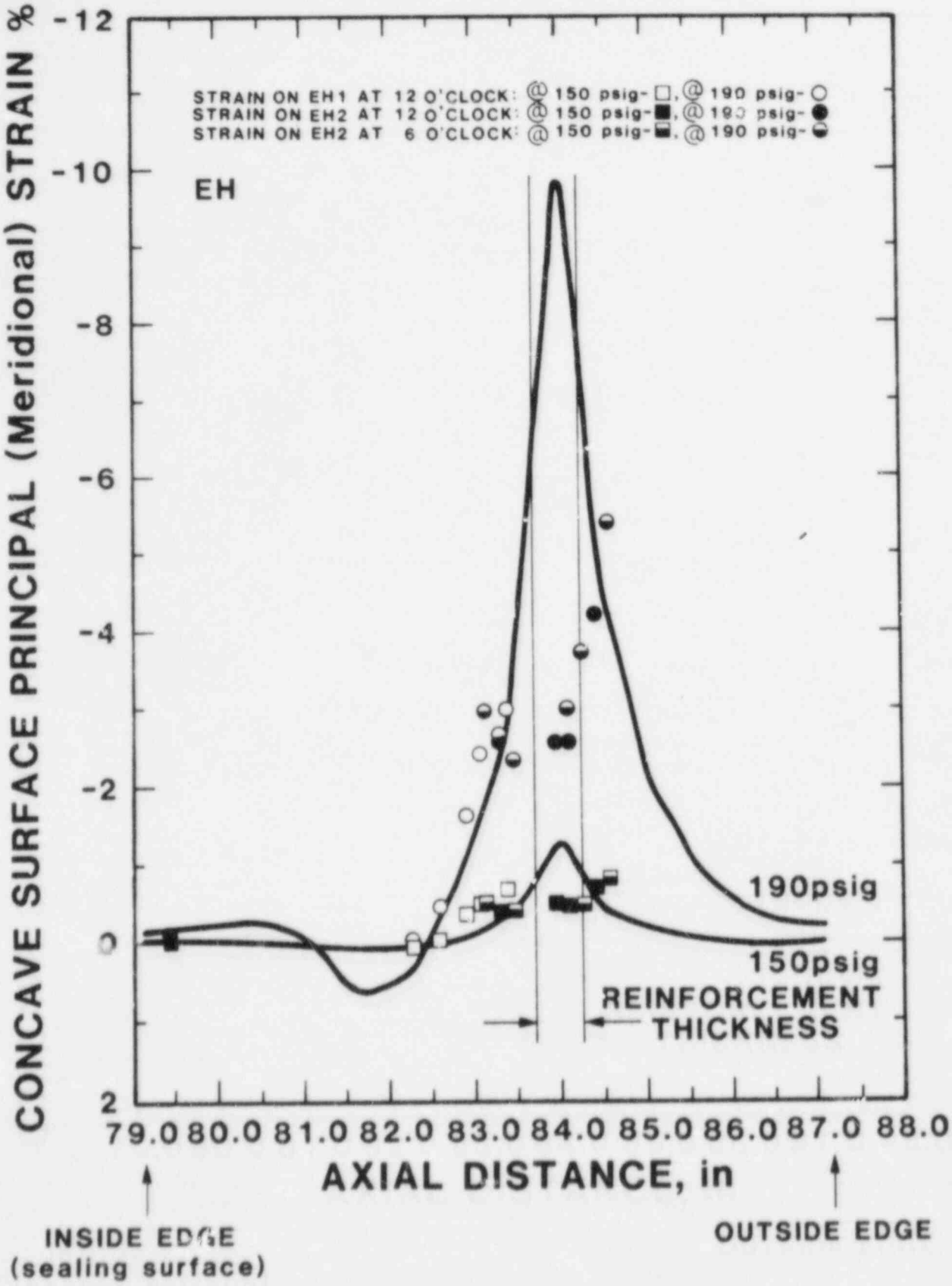

Figure 23 Variation in Meridional Strain Along EH Sleeves at 6 and 12 O'clock

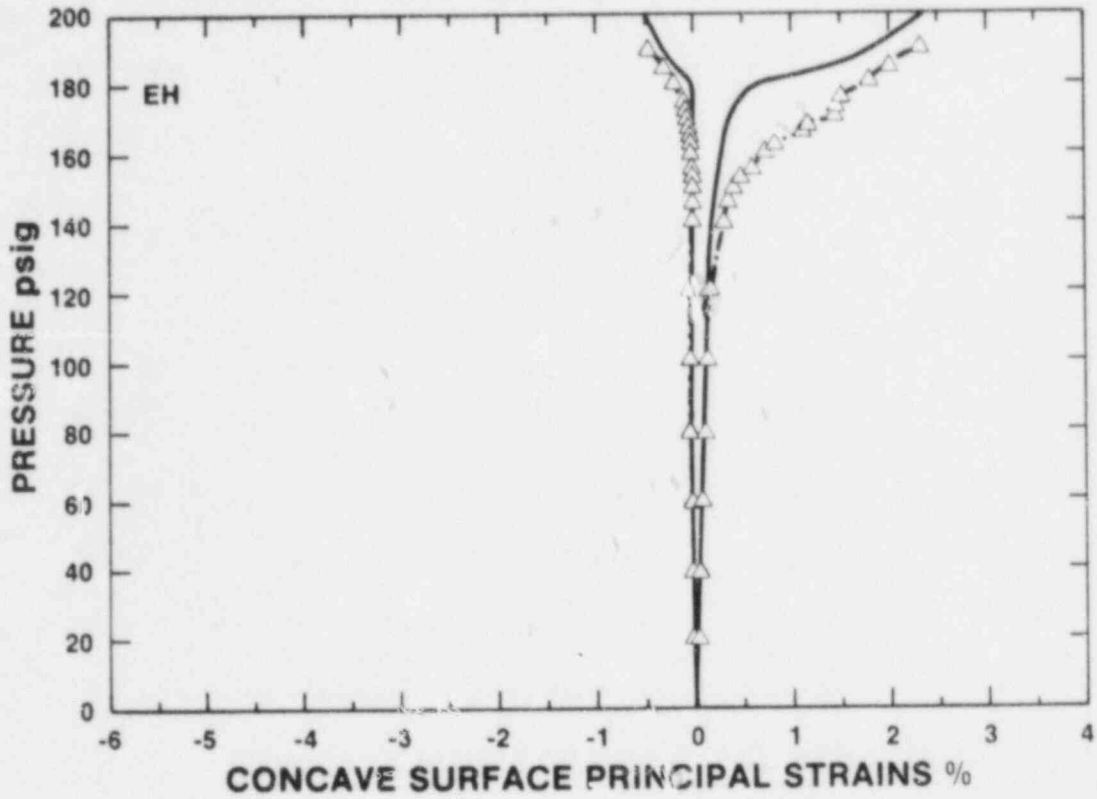

Figure 24 EH Sleeve Strains at 12 O'clock 1.4" Inward

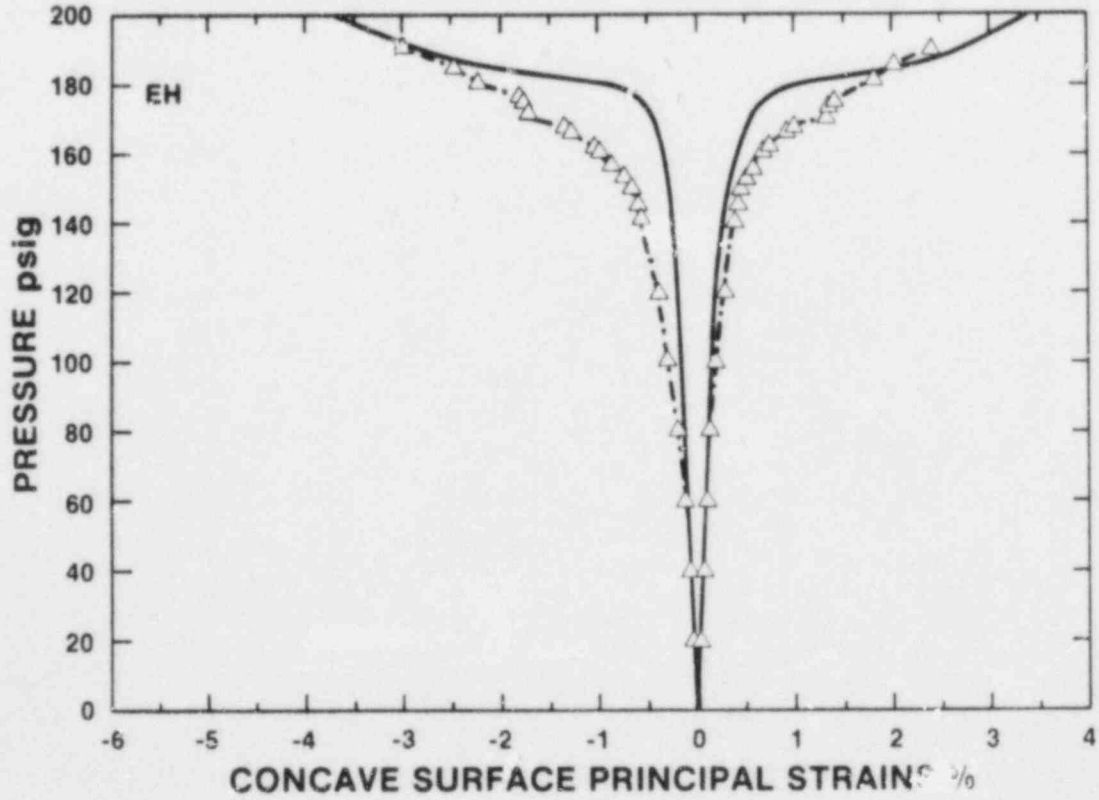

Figure 25 EH Sleeve Strains at 12 O'clock C.6" Inward

At the 3 and 9 o'clock positions on the sleeve, the strains were relatively small along the entire length, as shown in Figure 26. Pressure histories of the strain on the sleeve of equipment hatch 1 at 3 o'clock are shown in Figures 27 and 28 for two points along the length. Again, the agreement is exceptional.

7.3 Cover Response

The covers and their tensioning rings exhibited linear, elastic behavior during the course of the test, as expected. For many actual containments, buckling of the equipment hatch cover is expected to occur at relatively low pressure (but greater than the design pressure). In the 1:32-scale penetration model (SC3), the equipment hatch cover buckled at 50 psig. However, the equipment hatch covers in the 1:8-scale model were roughly twice as thick as they would have been had they been scaled from a prototypical containment, and consequently, buckling was not a concern. The critical pressure for elastic buckling was calculated using both finite element methods and handbook formulas to be over 3000 psig. The predicted response of the cover and tensioning ring was elastic up to 360 psig.

8. OTHER PENETRATIONS

The other penetrations in the model were not as heavily instrumented as the equipment hatches. A limited number of strain rosettes were used on the personnel lock sleeves and the constrained pipe. This instrumentation is shown schematically in Figure 29. No unexpected behavior was observed. Bending resulted in large strains near the sleeve's intersection with the reinforcement, and away from the intersection, strains were very small, in many cases remaining elastic throughout the test. The strains on the constrained pipe were very small along its entire length, although they did increase at its intersection with the reinforcement at 12 o'clock, as shown by Figures 30 and 31. Strains recorded on the sleeve of personnel lock 2, Figures 32 and 33, demonstrate again the significant difference between the magnitudes of the strains at 6 and 12 o'clock, and those at 3 and 9 o'clock.

9. REINFORCEMENTS

The instrumentation on the reinforcements around penetrations is shown in Figure 34. In general, the strains recorded with these gages were small compared to the membrane strains in the cylinder, as shown in Figure 35. However, a few rosettes that were located on the reinforcement immediately adjacent to the intersection with the penetration sleeves did record unexpectedly large strains. In particular, the strains in the reinforcement just above SF2, Figure 36, were much larger than predicted. The mesh refinement for the reinforcements was not sufficient to accurately model the bending response at these

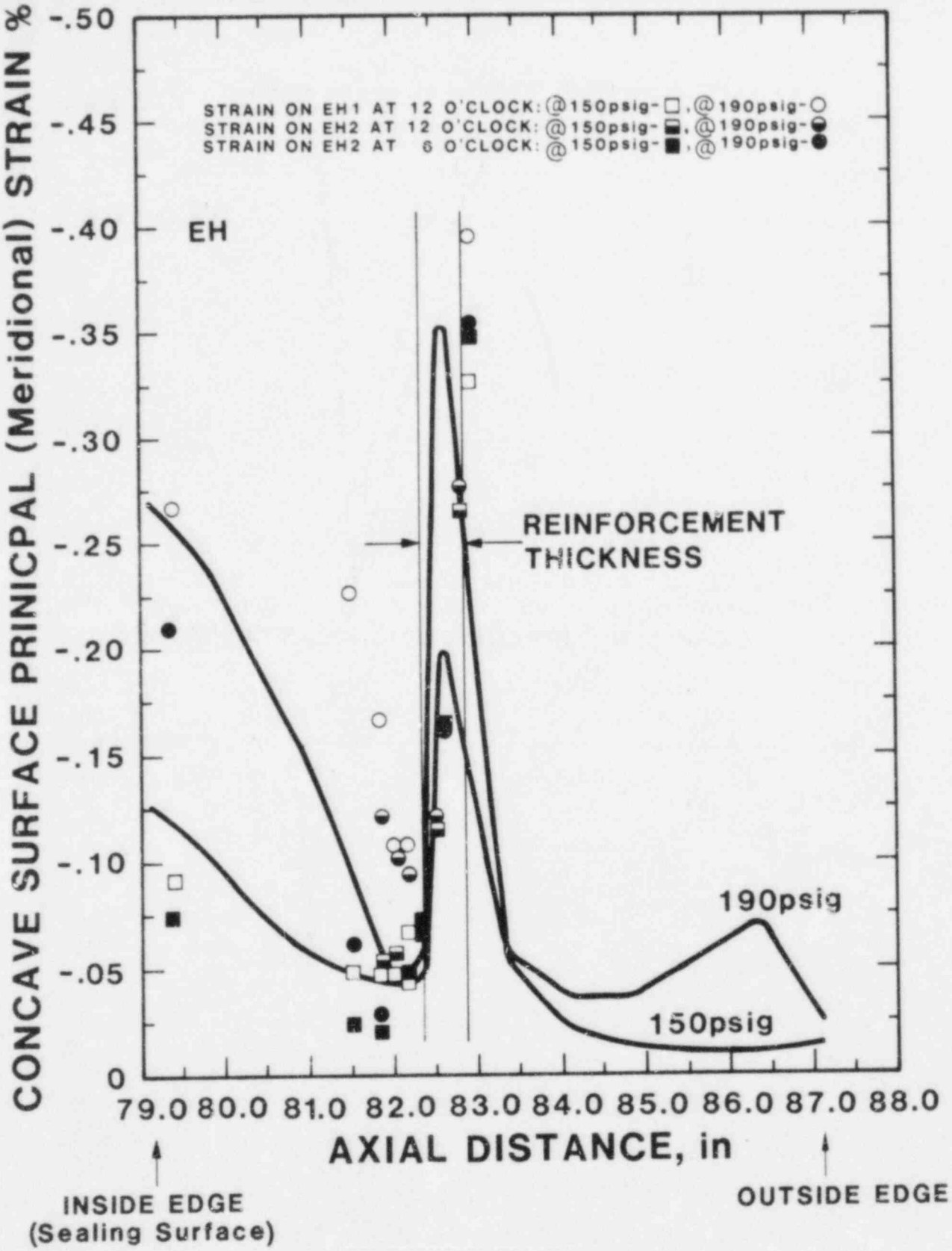

Figure 26 Variation in Meridional Strain along EH Sleeves at 3 and 9 O'clock

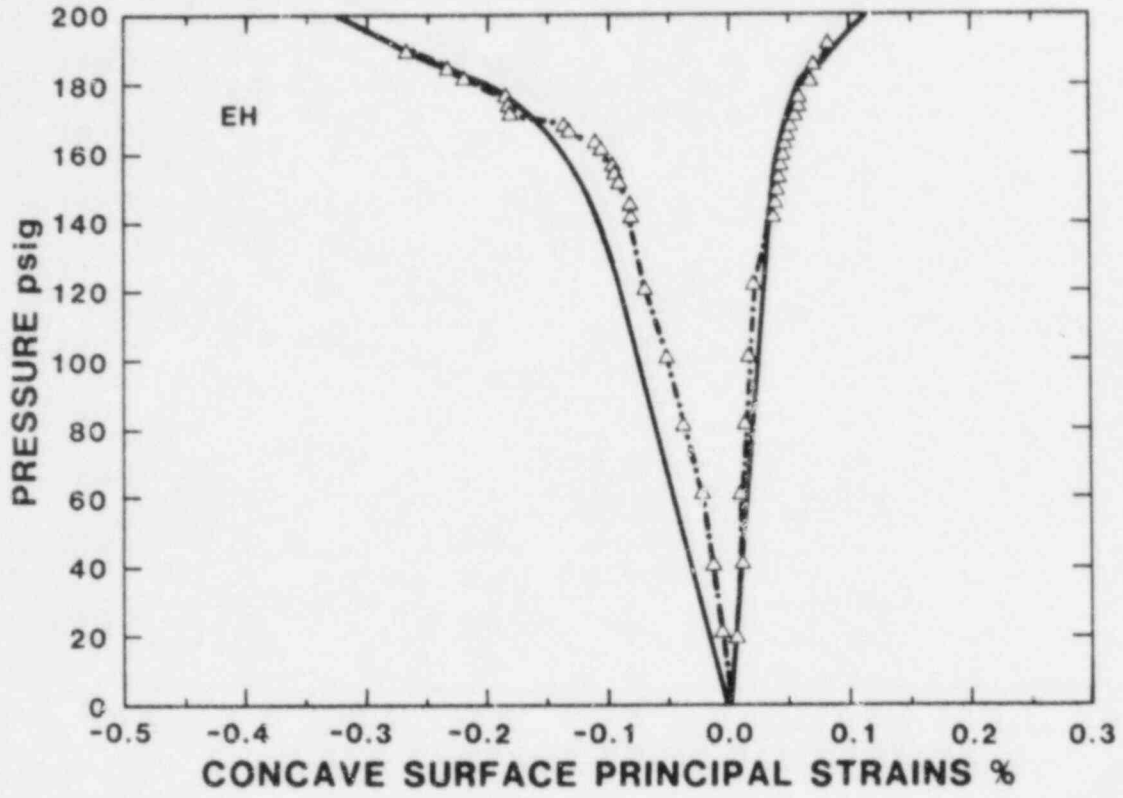

Figure 27 EH Sleeve Strains at 3 O'clock 2.7" Inward

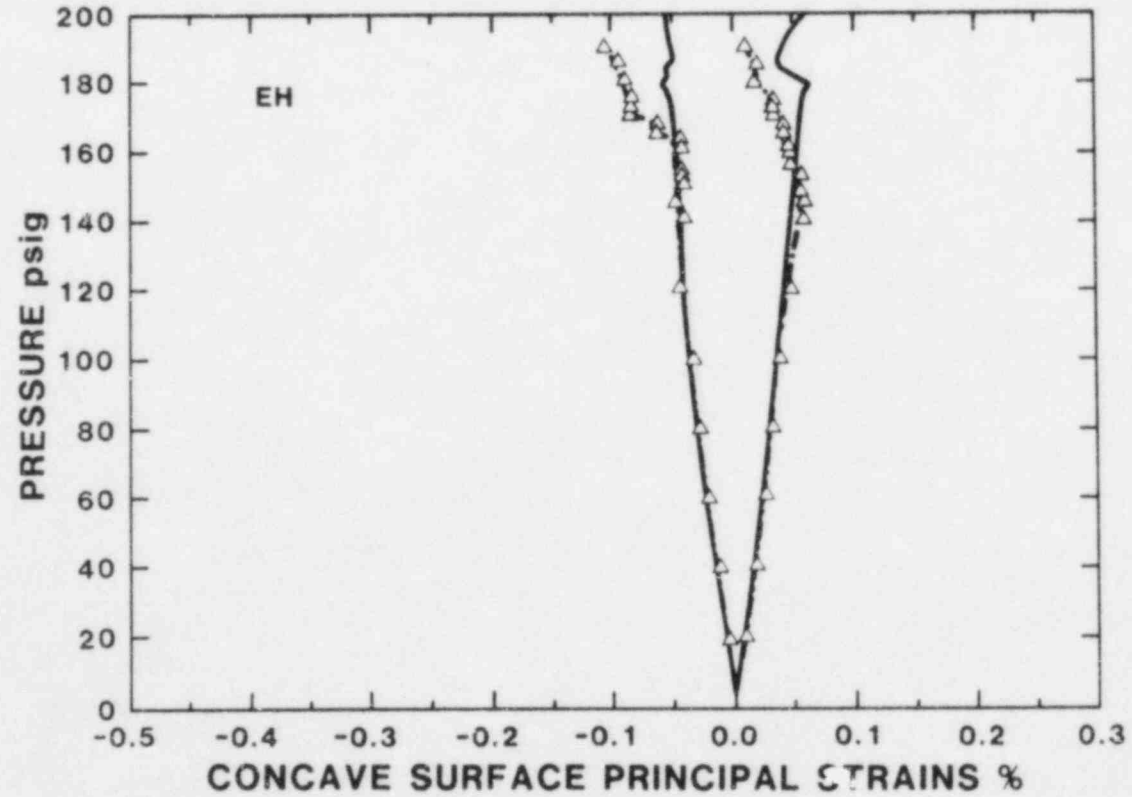

Figure 28 EH Sleeve Strains at 3 O'clock 0.5" Inward

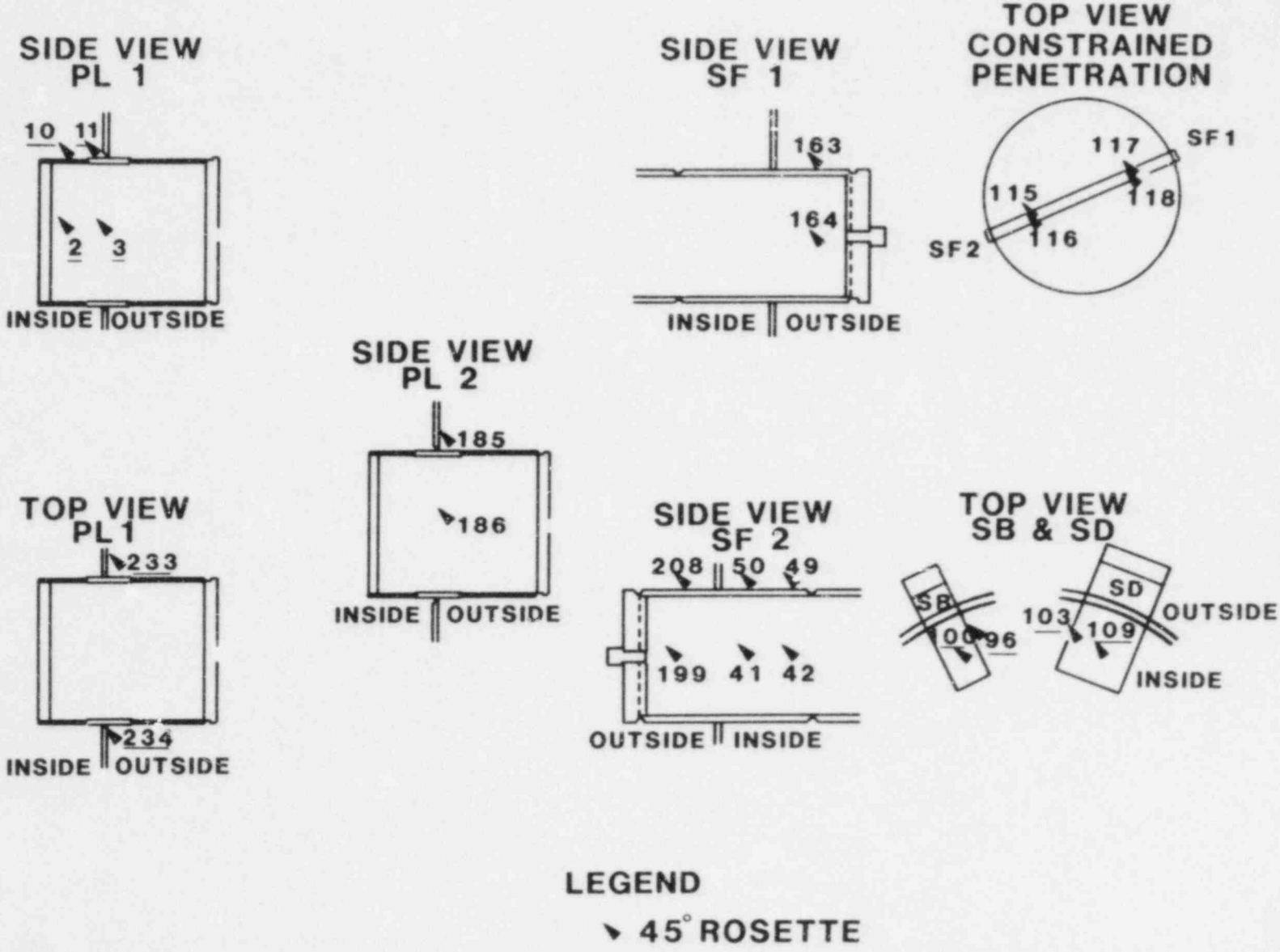

Figure 29 Schematic of Instrumentation on Penetration Sleeves Other than the Equipment Hatch Sleeves

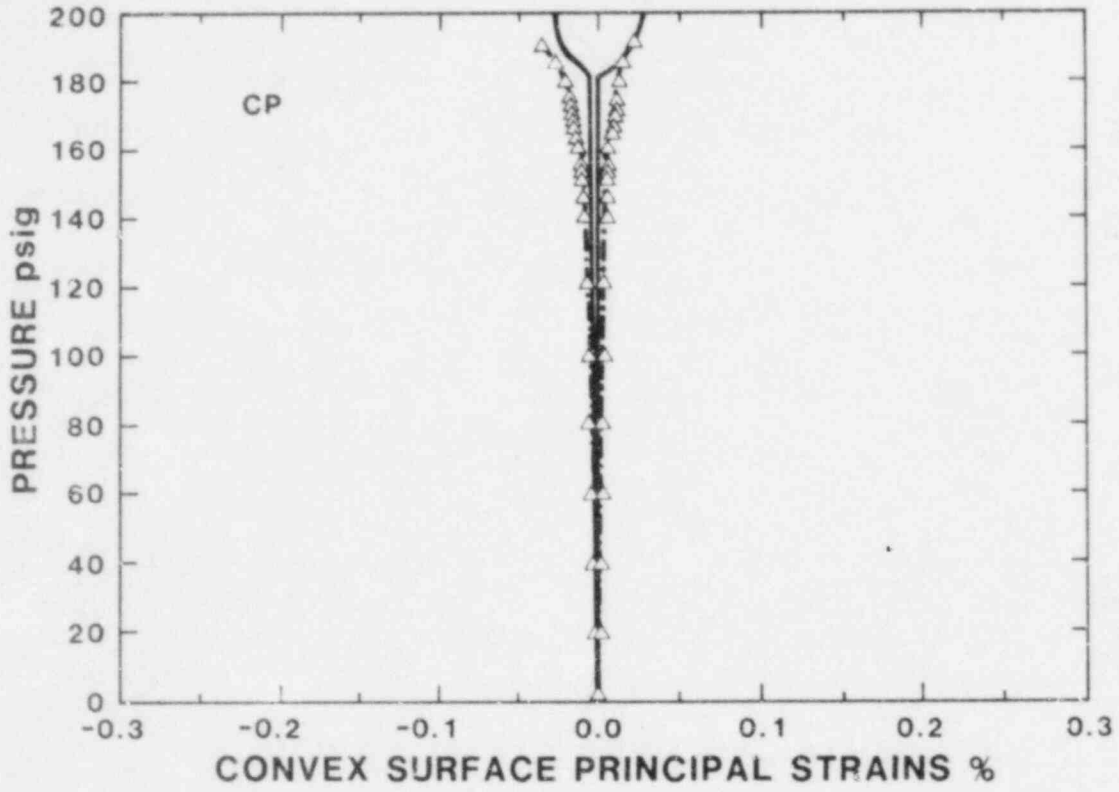

Figure 30 SF2 Sleeve Strains at 12 O'clock 5" Inward (SG 49)

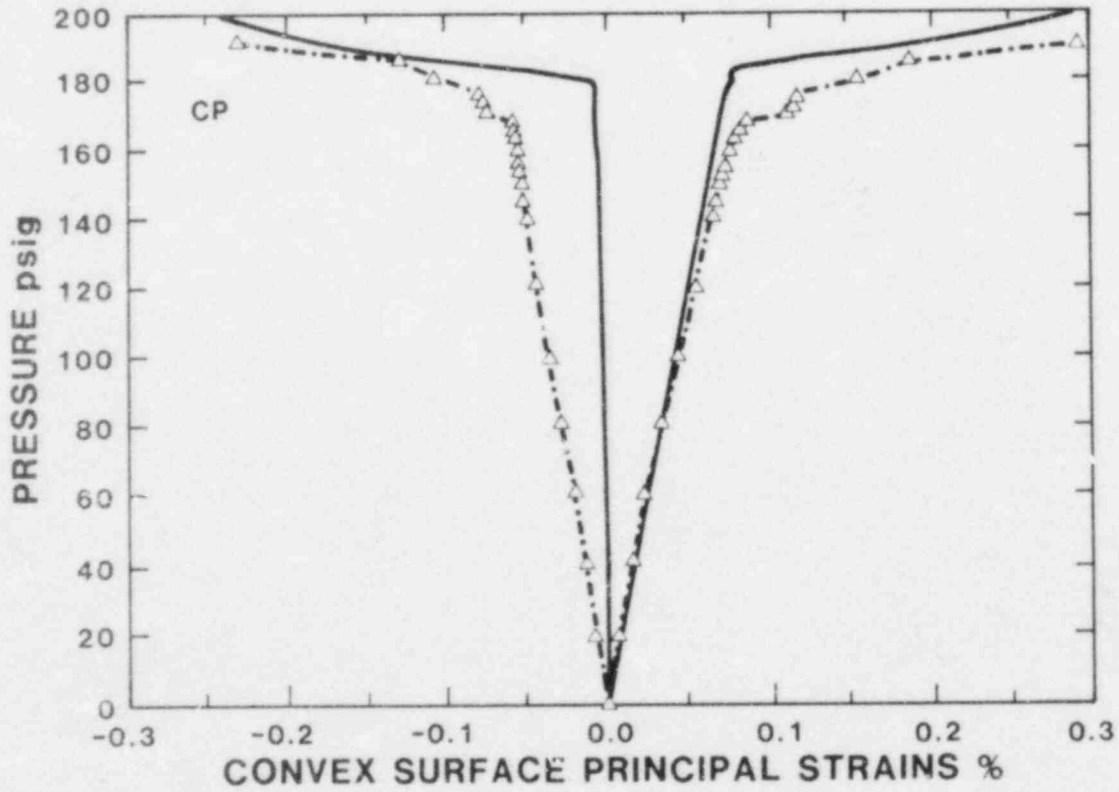

Figure 31 SF2 Sleeve Strains at 12 O'clock 1" Inward (SG 50)

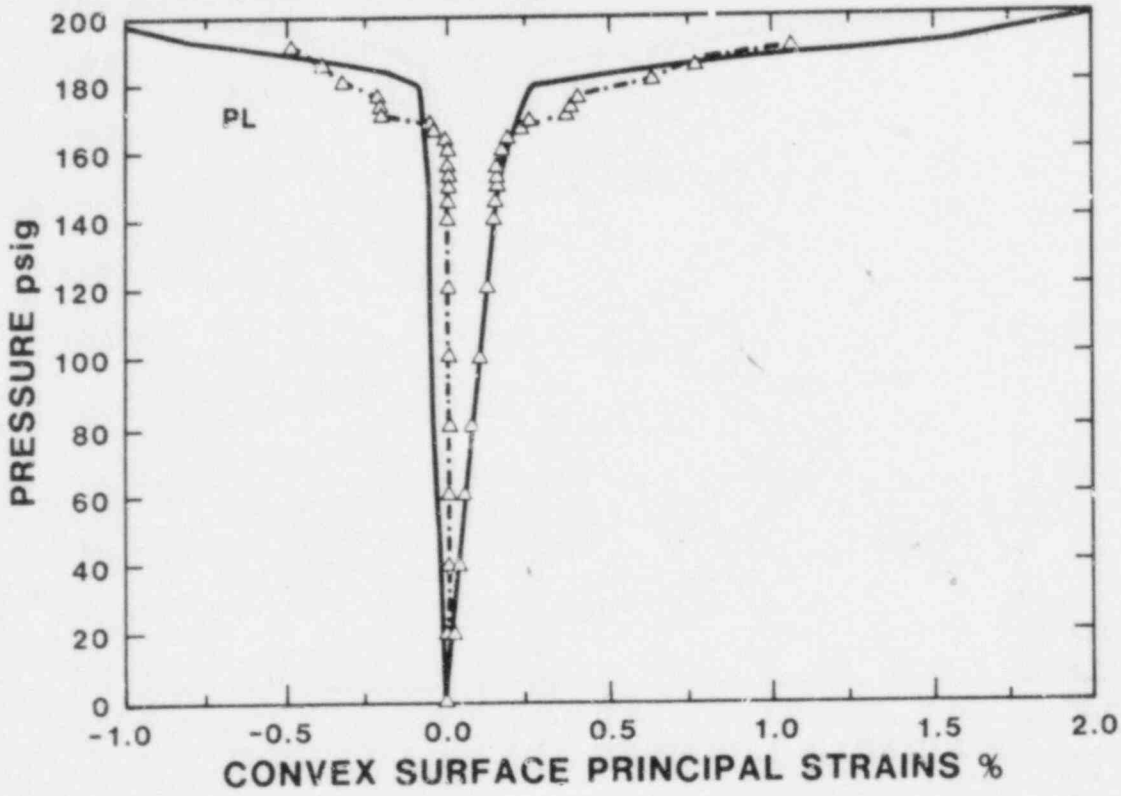

Figure 32 PL2 Sleeve Strains at 12 O'clock 0.8" Out (SG 185)

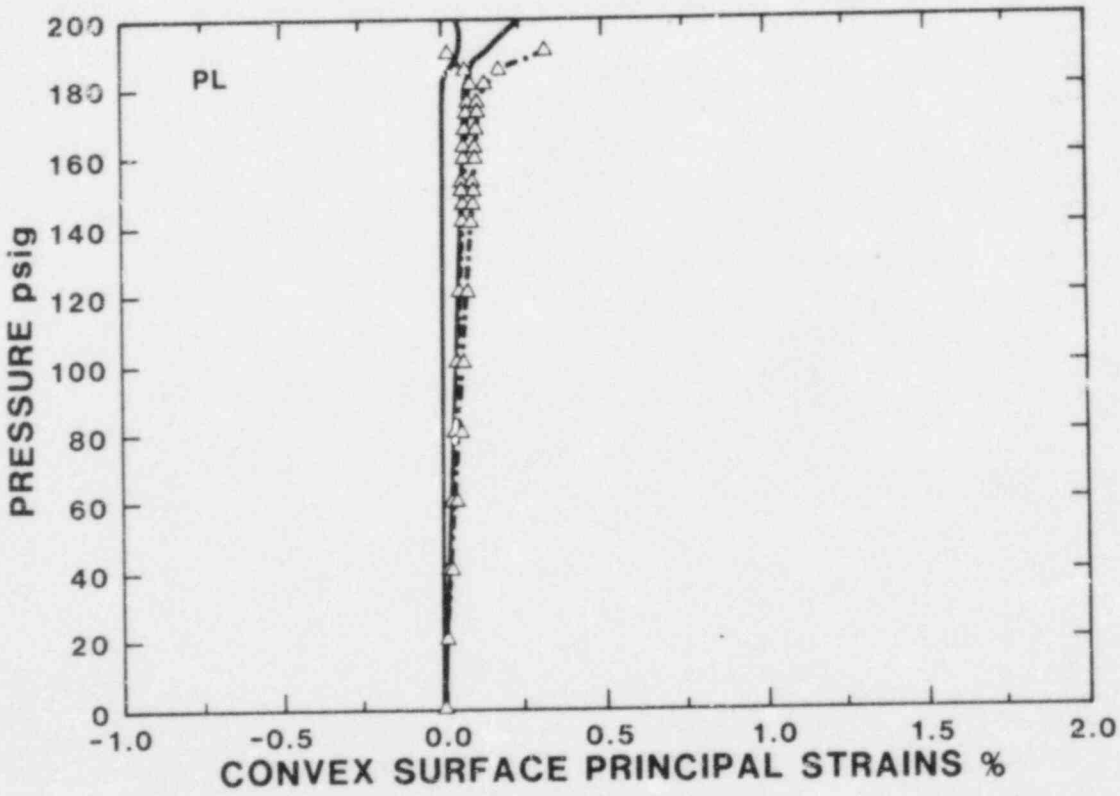

Figure 33 PL2 Sleeve Strains at 3 O'clock 0.8" Out (SG 186)

GAGES ON INTERNAL SURFACE VIEWED FROM OUTSIDE

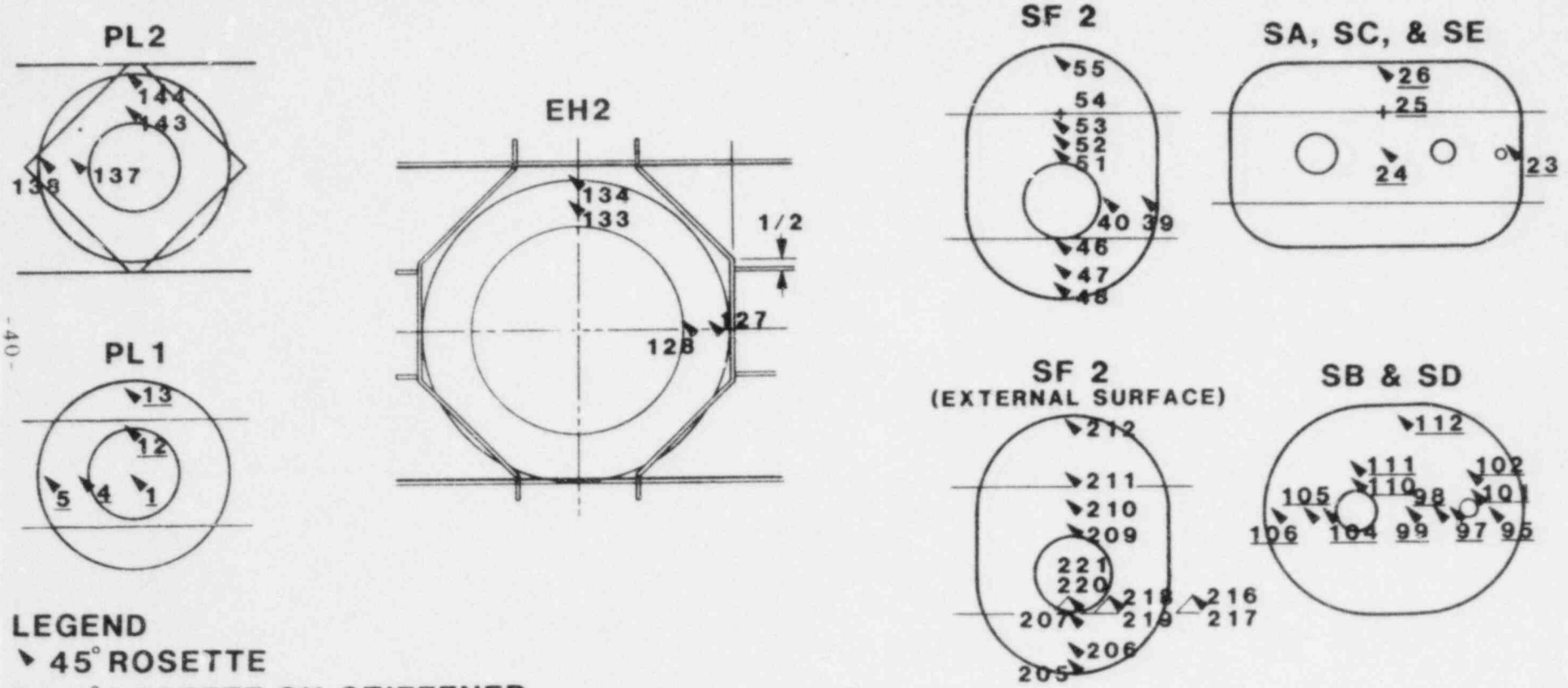

Figure 34 Schematic of Instrumentation on Reinforcements

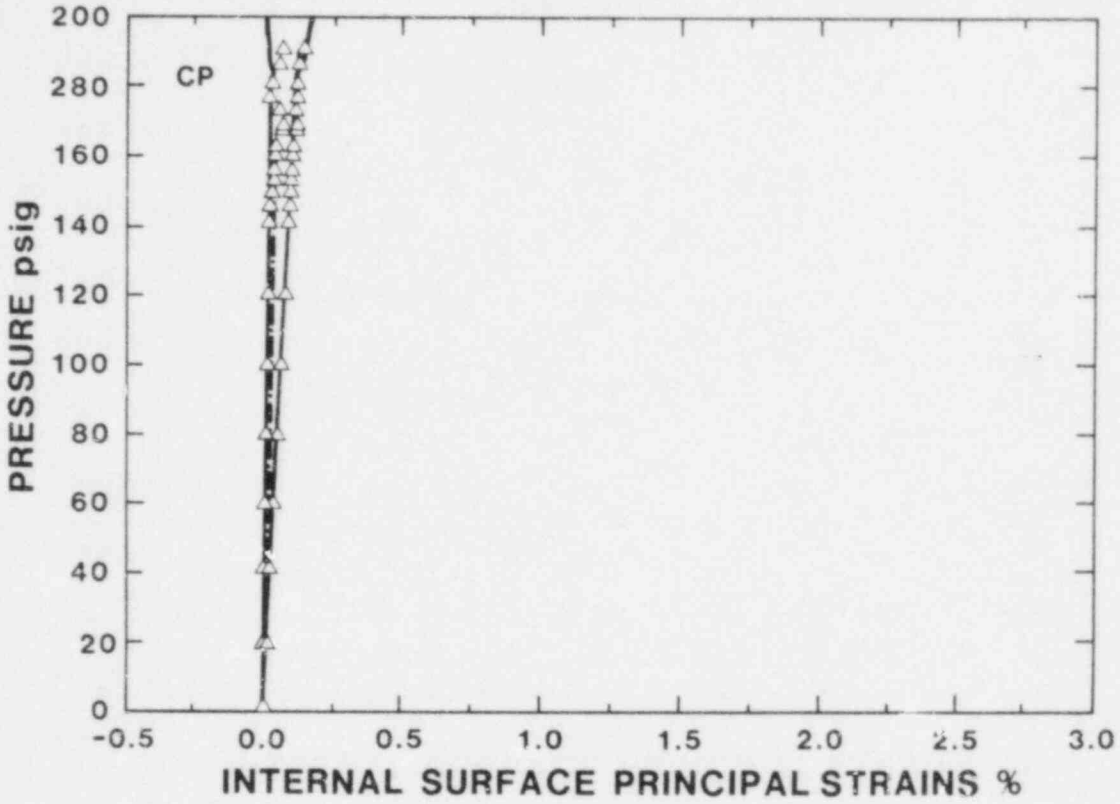

Figure 35 SF2 Reinforcement Strains vs. Pressure (SG 39)

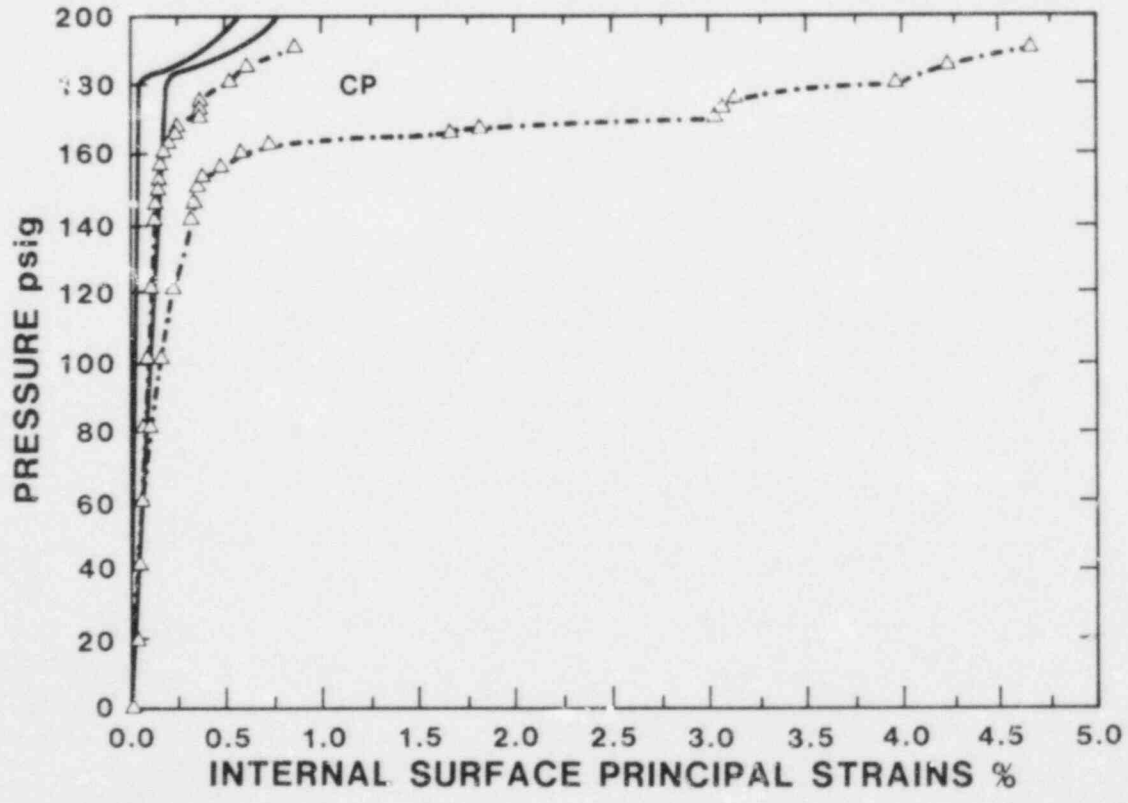

Figure 36 SF2 Reinforcement Strains vs. Pressure (SG 51)

locations. High bending strains in the reinforcements were not anticipated because of the increased thickness of these areas.

10. EVALUATION OF ANALYTICAL METHODS

The analysis of a nuclear containment subject to loads arising during a severe accident can be divided into two distinct steps. The first step consists of solving for the strains and displacements at different pressure (and temperature) levels. Implicit in this first step is an analyst's ability to identify which sections of the containment are critical and the amount of detail that must be included in an analytical model to obtain accurate results. The next step consists of inferring structural performance (by evaluating criteria for leakage and rupture) from the predicted strains and displacements in the model, as well as other parameters, such as thermal and radiation aging of seals, and aerosols.

10.1 Predicting Strain and Displacement

Strains and displacements can be predicted with reasonable accuracy using available analytical methods. Most discrepancies between predictions for the 1:8-scale steel model and the experimental results were the result of fabrication and strain rate effects on the material properties. More precise predictions could have been obtained by modifying the uniaxial material properties to account for these effects. For instance, the yield stress input to the code could have been reduced 10% to account for anticipated strain rate effects and the Bauschinger effect. Some differences, in particular for bending strains in reinforcements and in the formed stiffener around the equipment hatches, were the result of a lack of detail in the finite element models. An analyst using finite element methods must be able to anticipate the various locations and types of response that can be encountered in shells in order to design a mesh that can be used to accurately calculate the containment response. Localized behavior can have important consequences on the overall containment behavior, as demonstrated by the outcome of the scale model test. In particular, any area where there is a potential breakdown of the membrane load carrying action of the structure should be carefully analyzed. Given an accurate characterization of the geometry and a sufficiently refined mesh, the response of even complex parts of a steel containment can be predicted with reasonable accuracy by finite element methods.

10.2 Structural Performance

Additional work is needed to refine and verify reliable leakage and rupture criteria. Leakage criteria for penetrations that have not yet been analyzed or tested will be proposed. The preliminary leakage criteria are limited to predicting the onset of leakage; they will be extended so that leak rates can be predicted. The application of these criteria, especially for leakage, will probably require additional calculations (beyond

the structural analyses used to predict strain and displacement), and they will definitely require sound engineering judgement. Accuracy in the predictions for structural performance of steel containments is limited by the accuracy of the method used to predict the relevant parameters (primarily strain and displacement) used in the leakage and rupture criteria.

The leakage criterion for equipment hatches with pressure seating seals (the onset of leakage was assumed to occur when the local radial deformation of the sleeve relative to the cover exceeded the effective thickness of the sleeve at the seal surface) was probably a good first approximation. Additional work is needed to predict leak rates as the pressure, or temperature, or both continue to increase after the onset of leakage. Because leakage thru penetrations depends on deformation, it is not as sensitive to highly localized structural phenomena as rupture. An experimental program which addresses the leakage potential for a number of different penetrations and seal types and geometries is in progress [12,13]. This program will provide information on seal degradation due to thermal and radiation aging and its effect on leakage, and the potential for plugging of leakage paths by aerosols.

In the light of results of the post-test analysis, the rupture criterion that was used for the 1:8-scale model appears to be reasonable (rupture was predicted to occur when the maximum equivalent strain was equal to the uniaxial tensile strain at maximum load). Alternative rupture criteria are not available. For instance, fracture mechanics approaches have not developed to the stage where they can address ductile failure in a complex structure. However, because there is no experimental data which directly validates the criterion (no strain measurements were obtained in the 1:8-scale model immediately adjacent to the initial fracture surface), and because the criterion is not based on first principles (it is empirical), it must be subject to further scrutiny and evaluation. It is recognized that, in the high strain regimes, the uncertainty in the predictions is large, but it is necessary to analyze the response to these levels in order to determine whether the containment fails by leakage or rupture.

A more difficult problem confronting rupture predictions is that rupture is often caused by highly localized phenomenon that may be difficult to anticipate. When oversights occur, nonconservative estimates for the strength of the containment can result. An alternative approach to predicting strength that avoids such difficulties would be to predict strains and displacements with relatively simple models and use a very conservative criterion to predict rupture, such as associating rupture with membrane yield of the cylinder. The disadvantage of this approach is that it could lead to misleading estimates of risk by favoring one possible failure mode (rupture) over another (leakage).

10.3 What is "Good Enough"?

An important question that arises is what level of analysis of containment buildings subject to severe accidents is needed to obtain results which are useful and meaningful to consequence analyses, such as probabilistic risk assessments (PRAs). Uncertainties abound, from the temperatures and pressures arising from a severe accident, to the evaluation of risk. As stated in the introduction, the capacity of the containment, and the timing, mode, and location of a failure are basic inputs to a consequence analysis. Order of magnitude predictions for leakage rate could be used to further differentiate risk. The level of analysis that will be required to provide these answers will depend largely on the results of investigations into the leakage characteristics of containment penetrations that are now in progress [12,13]. If these studies identify penetrations or seal geometries that are likely to leak prior to the onset of membrane yielding, the structural analyses of containments to be used for consequence analyses can be relatively simple. However, preliminary indications are that leakage from penetrations will not occur below the membrane yield pressure. If this is the case, predictions for leakage and rupture would require structural analyses to be carried out to pressures greater than the membrane yield pressure, and the analyses would therefore be similar in complexity to those conducted for the 1:8-scale steel model.

In either case, the differences between individual containment building designs for LWR's are substantial, and therefore, a consequence analysis for a containment should be based on detailed structural analyses of that containment. The tests on the steel scale models have demonstrated that the structural behavior of steel containments can be predicted with finite element methods, including both elastic and nonlinear (including large displacement and finite strain) response.

Exact and approximate closed form solutions could be investigated as a possible alternative or supplement to finite element analyses. If a highly conservative rupture criterion is adopted, or if research shows that some penetrations will leak before membrane yielding begins, these methods could be competitive with finite element methods. Some approximate methods developed based on the finite element analyses of the 1:8-scale model seem to work well, for instance, calculating the deformation of the equipment hatch sleeve from the average strain in the cylinder closely matched the experimental data. However, it is unlikely that any approach other than finite element methods can be used to accurately and quantitatively predict the response near complex intersections and connections.

Finite element methods are the best tool currently available for conducting structural analyses of containments subject to severe accident loads. Accurate results rely on the ability of an analyst to identify the critical areas of the containment: The scale model tests have provided invaluable insight into how and where the crucial areas are found. In particular, locations

where there is a possibility of a breakdown in the membrane load carrying action of the structure should be carefully analyzed. The effect of major penetrations on the response also has to be considered. If finite element models are sufficiently detailed, accurate results will be obtained, and rupture criterion based on the uniaxial tensile strain at maximum load will yield reasonable results. When leakage criteria for all penetrations and seal geometries are completed, predictions for containment behavior during a severe accident that can be used confidently in consequence analyses will be possible.

11. REFERENCES

[1] CLAUSS, D.B., "Pretest Predictions for the Response of a 1:8-Scale Steel LWR Containment Building Model to Static Overpressurization," NUREG/CR-4137, SAND85-0175, Sandia National Laboratories, Albuquerque, NM, June 1985.

[2] CLAUSS, D.B., and HORSCHEL, D.S., "Comparisons of Analytical and Experimental Results from Pressurization of a 1:8-Scale Steel Containment Model," Proceedings 8th Intl. Conf. on Structural Mechanics in Reactor Technology, Brussels, Belgium, August 19-23, 1985, Paper J 2/5.

[3] VON RIESEMANN, W.A., et al., "U.S. NRC Containment Integrity Programs," Proceedings 8th Intl. Conf. on Structural Mechanics in Reactor Technology, Brussels, Belgium, August 19-23, 1985, Paper J 1/2.

[4] HORSCHEL, D.S., "The Design, Fabrication, Testing and Analyses of Four 1:32-Scale Steel Containment Models," NUREG/CR-3902, SAND84-2153, Sandia National Laboratories, Albuquerque, NM, (to be published).

[5] REESE, R.T. and HORSCHEL, D.S., "Design and Fabrication of a 1:8-Scale Steel Containment Model," NUREG/CR-3647, SAND84-0048, Sandia National Laboratories, Albuquerque, NM, (February 1985).

[6] MARC General Purpose Finite Element Program, Revision K.1, MARC Analysis Research Corp., Palo Alto, California, 1983.

[7] BLEJWAS, T.E., "Internal Pressure Experiments with Steel and Concrete Containment Models," Proceedings 8th Intl. Conf. on Structural Mechanics in Reactor Technology, Brussels, Belgium, August 19-23, 1985, Paper J 2/3.

[8] KOENIG, L.W., "Techniques and Results from the Internal Pressurization of a 1:8-Scale Steel Containment Model," Proceedings 8th Intl. Conf. or Structural Mechanics in Reactor Technology, Brussels, Belgium, August 19-23, 1985, Paper J 2/4.

[9] CLAUSS, D.B., "Summary of Pretest Predictions for the 1:8-Scale Steel Containment Model," Internal Memorandum to T.E. Blejwas, Sandia National Laboratories, Albuquerque, NM, November 9, 1985.

[10] KOENIG, L.M., "The Test of a Large Steel Containment Model", NUREG/CR-4216, SAND85-0790, Sandia National Laboratories, Albuquerque, NM, (to be published).

[11] CHIAPPETTA, R.L., "Review of IITRI Reports on Stuctural Studies of Reactor Containment," CWA Project 4017, Purchase Order 59-3974, Chiapetta, Welch and Associates, Ltd., 9748 Roberts Road, Palos Hills, IL 60465, (April 1985).

[12] SUBRAMANIAN, C.V., "Integrity of Containment Penetrations Under Severe Accident Loadings," Proceedings of the 8th Intl. Conf. on Structural Mechanics in Reactor Technology, Brussels, Belgium, August 19-23, 1985, Paper J 4/2.

[13] SUBRAMANIAN, C.V., "Integrity of Containment Penetrations Under Severe Accident Conditions - FY84 Annual Report," NUREG/CR-4119, SAND85-0016, Sandia National Laboratories, Albuquerque, NM, (to be published).

APPENDIX A
POST-TEST FINITE ELEMENT ANALYSIS OF THE FORMED STIFFENER

In an effort to understand why the 1:8-scale model failed differently than predicted, a finite element analysis was conducted with a more refined mesh than that used prior to the test. The model ruptured at 195 psig: It is believed that the failure initiated in the formed stiffener just below its juncture with circumferential stiffener 7, and then propogated into the shell wall. Examination of the fragments showed that cracks had also occurred in the formed stiffeners at each of the seven other geometrically symmetric locations. (There were four junctions between formed stiffeners and circumferential stiffeners for each of the two equipment hatches.) Metallurgical investigations have demonstrated that the fracture was ductile, and there was no degradation of the material properties in the vicinity of the weldment. High strains were not predicted at the juncture of the stiffeners with the pretest analysis. Initially, the validity of the rupture criterion was suspected. It was thought that the high degree of constraint at the weldment, and the complex state of stress could have resulted in a failure at strains below the uniaxial tensile strain at maximum load. However, a post-test analysis was conducted to determine if the strains in the formed stiffener were correctly predicted, and also to understand how and why the fracture propogated into the shell wall after the formed stiffener had cracked.

The post-test model is shown in Figure A1. The model consisted of 931 thin shell elements and 4856 active degrees of freedom. Since earlier analyses had shown that the maximum radial displacement of the cylinder occurred near the elevation of the equipment hatch, quarter symmetry was assumed, resulting in a considerable reduction in the size of the model. The small vertical extension of the formed stiffener below circumferential stiffener 7 was included in the model, unlike the pre-test model (see Figure 2 in the text). The size of the elements near the stiffener's juncture was much smaller than in the earlier analysis. Aside from these differences, the input and control of the pre- and post-test analysis were very similar.

Initial yielding of the model occurred in the formed stiffener just below its juncture with stiffener 7. The strain at this point increased steadily as shown in Figure A2, reaching 16% at 165 psig. At this point, the effect of a crack in the formed stiffener was introduced, by removing tying constraints between nodes on the formed stiffener and stiffener 7. (Due to the introduction of the crack, as the pressure was increased beyond 165 psig, the strain in the formed stiffener oscillated before settling on a constant value.) The maximum principal strain contours in the extension of the formed stiffener below stiffener 7 are shown in Figure A3. The strains are due primarily to bending. Due to the extension of the formed stiffener below stiffener 7, equilibrium at the juncture of the stiffeners cannot be satisfied by membrane forces alone, thereby resulting in significant bending moments. The results suggest the fracture

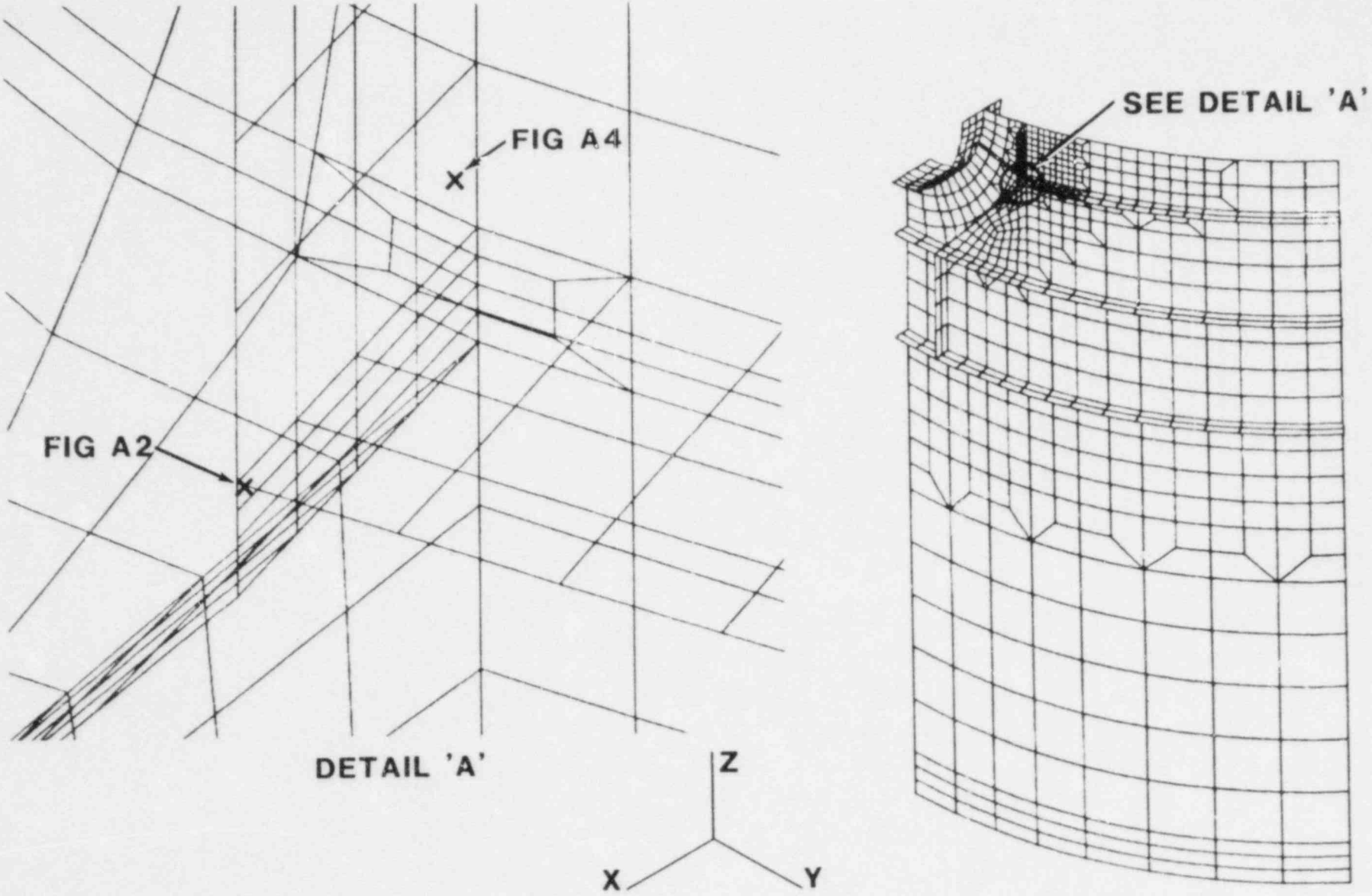

Figure A1 Finite Element Mesh for Post-Test Analysis

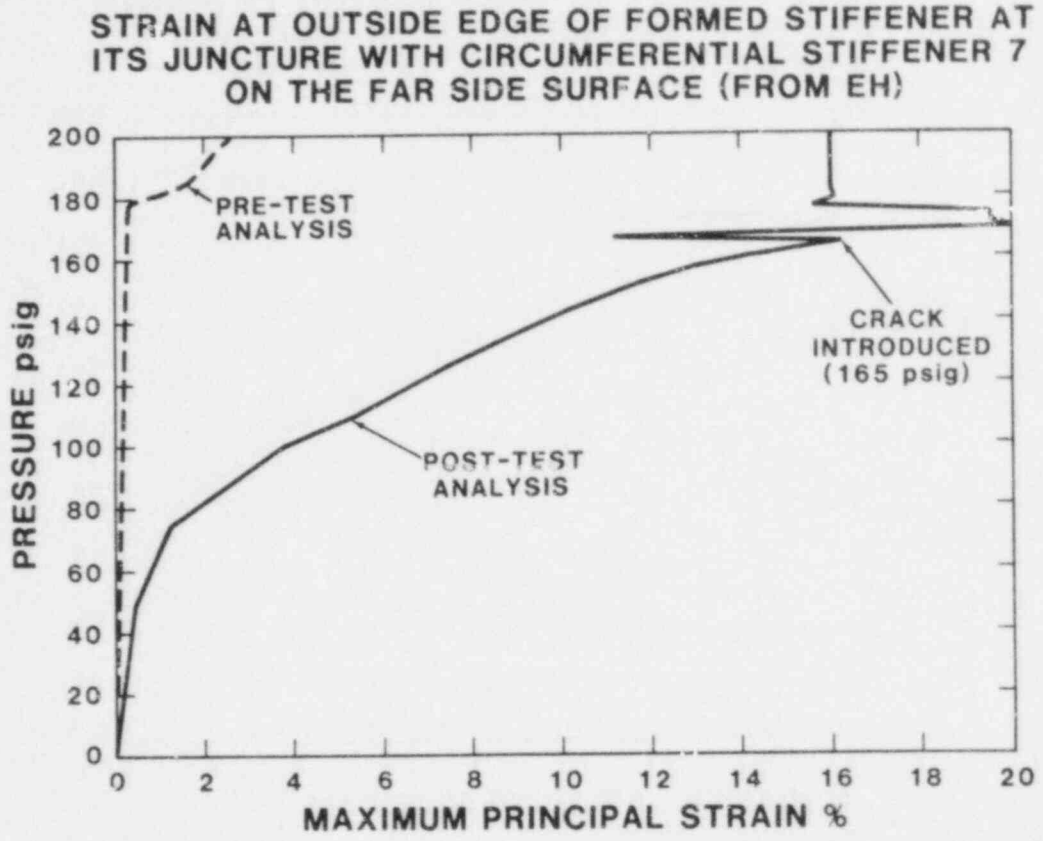

Figure A2 Maximum Principal Strain vs. Pressure in Formed Stiffener at its Juncture with Stiffener 7

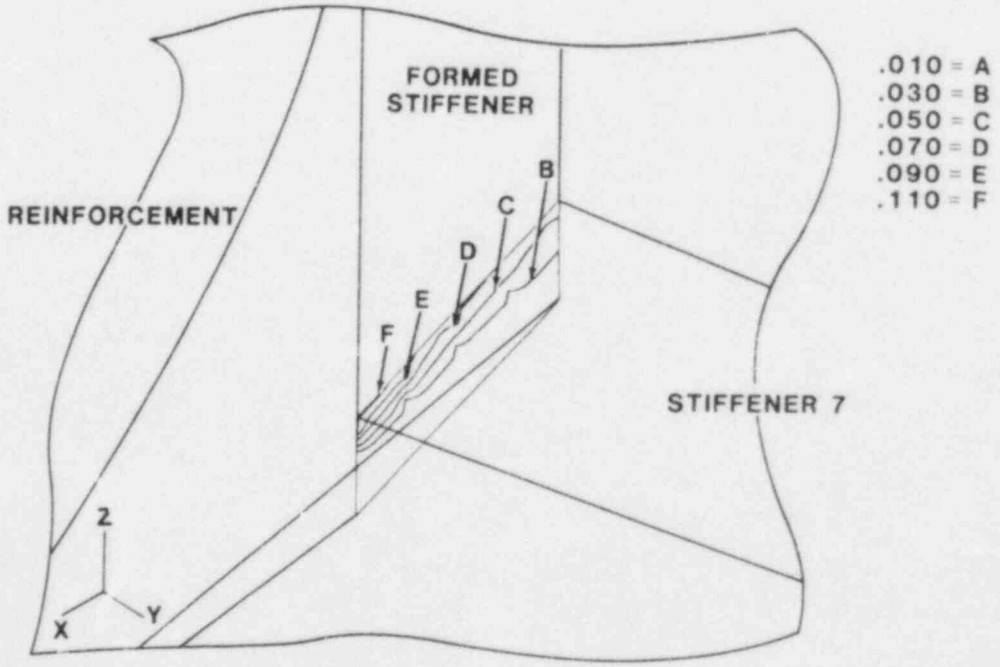

Figure A3 Maximum Principal Strain Contours in Extension of Formed Stiffener Below Stiffener 7

would have initiated on the outside edge of the stiffener and propogated thru the thickness and in towards the cylinder. This is consistent with the observations made by the theodolite operator who first noticed the crack at 165 psig.

The strain in the cylinder adjacent to the juncture of the stiffeners is shown in Figure A4 (see Figure A1 for the exact location). Because of the inefficiency of the geometry at the juncture of the stiffeners for carrying load, a very localized strain concentration occurred in the cylinder near the juncture. The strain reached 14.3% by 200 psig; the rupture criterion states that failure should occur at 15%. Because the actual yield stress for the cylinder material was less than the value used in the analyses (see Section 5), the actual strain in the cylinder at this point was almost certainly greater than the calculated value. This result for the strain in the cylinder suggests that the shell would have failed even if some means of arresting a crack in the stiffener had been designed, such as a 'rat' hole at the intersection of the welds between the stiffeners and the shell, and at the juncture of the stiffeners.

Comparisons between predictions and the post test analysis for the maximum principal strains at gages 154 and 151 are shown in Figures A5 and A6, respectively. Gages 154 and 151 were both at the elevation of equipment hatch 1, with gage 154 measuring the strain concentration in the cylinder adjacent to the reinforcement, and gage 151 measuring the "free-field" strain. Although the strains calculated with the pre- and post-test analyses are slightly different at gage 154, they are nearly identical at gage 151. This strongly suggests that the effect of the breakdown of membrane action at the juncture of the stiffeners was very localized.

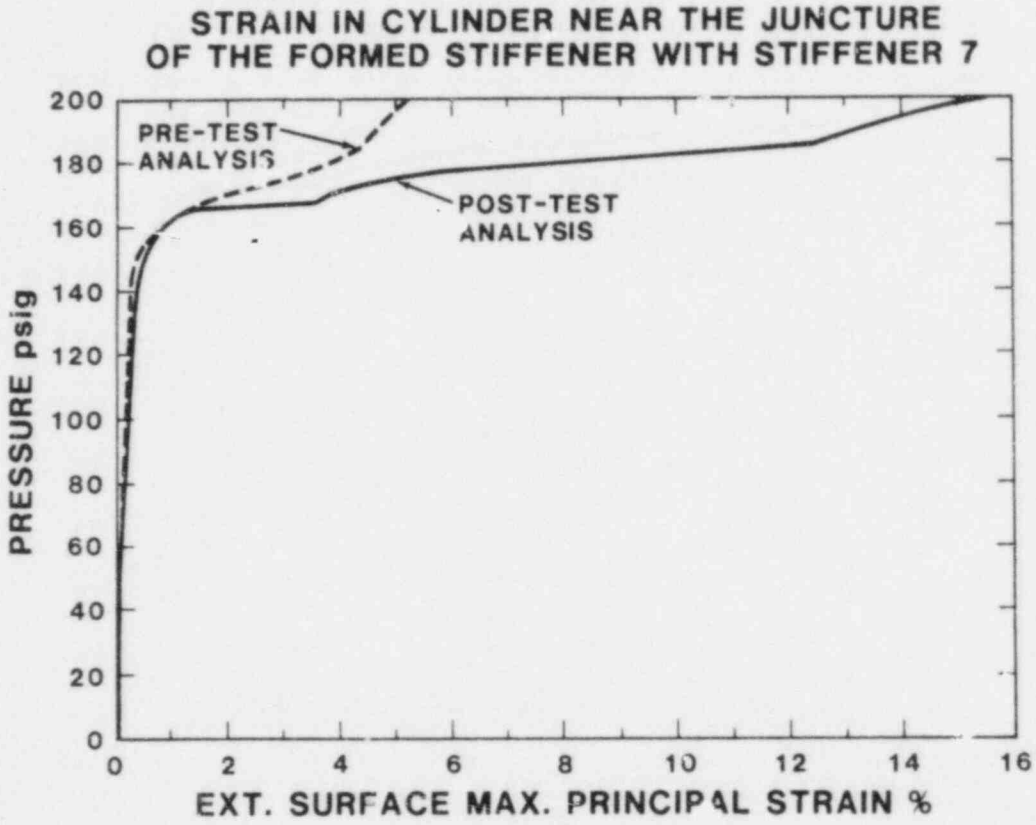

Figure A4 Maximum Principal Strain in Cylinder Near the Juncture of the Stiffeners

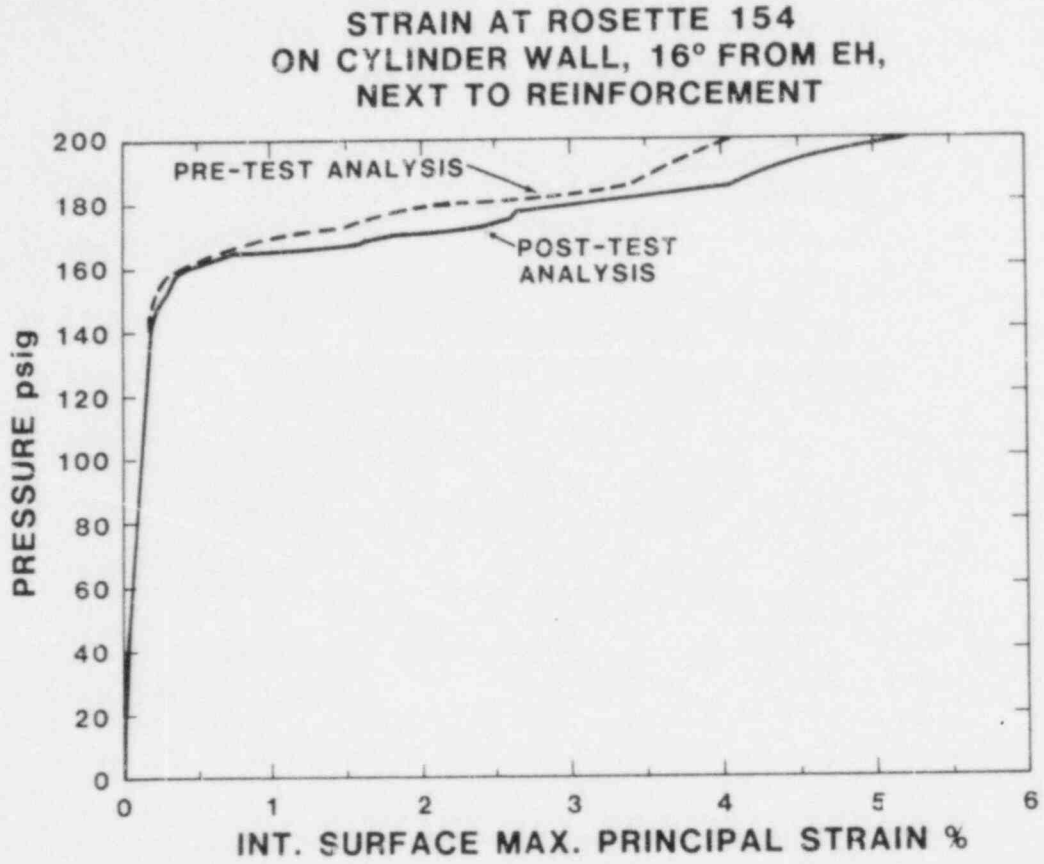

Figure A5 Maximum Principal Strain vs. Pressure at SG 154

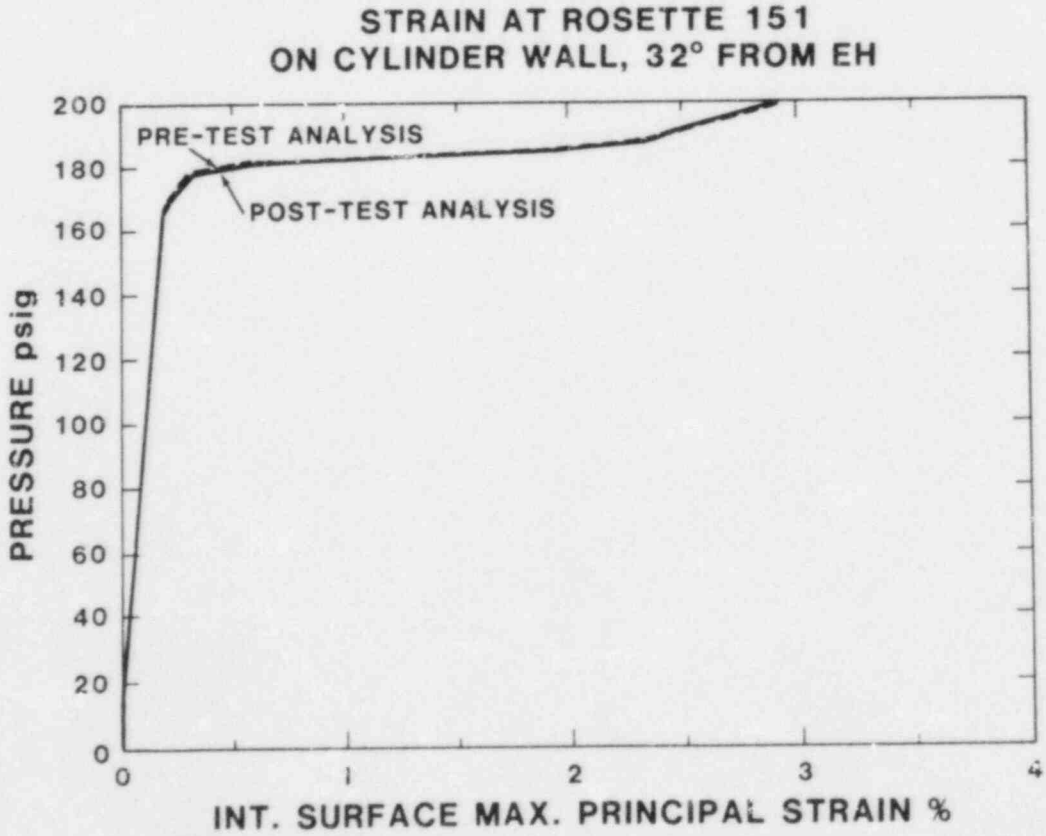

Figure A6 Maximum Principal Strain vs. Pressure at SG 151

APPENDIX B
MICROFICHE OF PLOTS COMPARING ANALYTICAL AND EXPERIMENTAL RESULTS FOR THE 1:8-SCALE STEEL MODEL

Distribution:

U. S. Government Printing Office
Receiving Branch (Attn: NRC Stock)
8610 Cherry Lane
Laurel, MD 20707 (385 copies for R1, RD)

US Nuclear Regulatory Commission
Division of Engineering Technology
5650 Nicholson Lane
Rockville, MD 20852
Attn: Hans Ashar (20 copies)

US Nuclear Regulatory Commission
Mechanical/Structural Engineering Branch
5650 Nicholson Lane
Rockville, MD 20852
Attn: J. F. Costello

John Clauss
NUTECH
225 W. Michigan Ave.
16th Floor
Chicago, Illinois 60601

Max H. French
M/C 901
General Electric Co.
175 Curtner Avenue
San Jose, CA 95125

Iowa State University
Department of Civil Engineering
420 Town Engineering Bldg.
Ames, IA 50011
Attn: L. Greimann

TVA
400 Commerce Ave.
Knoxville, TN 37902
Attn: D. Denton, W9A18

Los Alamos National Laboratories
PO Box 1663
Mail Stop N576
Los Alamos, NM 87545
Attn: C. Anderson

University of Illinois
Dept. of Civil Engineering
Urbana, IL 61801
Attn: C. Siess

University of Alberta
Dept. of Civil Engineering
Edmonton, Alberta, CANADA T6G 2G7
Attn: D. W. Murray

EBASCO Services, Inc.
Two World Trade Center
New York, NY 10048
Attn: J. J. Healdy, Consulting Engr.

Kernforschungszentrum Karlsruhe GmbH
Postfach 3640
D-7500 Karlsruhe
FEDERAL REPUBLIC OF GERMANY
Attn: R. Krieg, P. Gast (2 copies)

HM Nuclear Installation Inspectorate
Thames House North
Millbank, London, SW1
UNITED KINGDOM
Attn: R. J. Stubbs,
T. Currie (2 copies)

Mr. Thomas J. Ahl
Nuclear Design Group
Chicago Bridge & Iron Co.
800 Jorie Boulevard
Oak Brook, IL 60521

Dr. Wilfred E. Baker
Dept. of Ballistics & Exp. Sci.
Southwest Research Institute
6220 Culebra Rd.
PO Drawer 28510
San Antonio, TX 78284

William C. Black
2650 Woodside Road
Bethlehem, PA 18017

Ted M. Brown
Wiss, Janney, Elstner Assoc., Inc.
330 Pfingsten Road
Northbrook, IL 60062

P. A. Cox
Southwest Research Institute
6220 Culebra Road
P. O. Drawer 28510
San Antonio, TX 78284

Dr. Richard Denning
Battelle Columbus Laboratories
505 King Avenue
Columbus, Ohio 43201

Asadour H. Hadjian
Bechtel Power Corporation
12400 E. Imperial Highway
Norwalk, CA 90650

T. E. Johnson
Bechtel Power Corp.
777 East Eisenhower Pwy.
Ann Arbor, MI 48101

Bechtel Power Corporation
15740 Shady Grove Road
Gaithersburg, MD 20760
Attn: K. Y. Lee

Professor Mete A. Sozen
Dept. of Civil Engineering
University of Illinois
503 W. Michigan
Urbana, IL 61801

Dr. John D. Stevenson
Stevenson & Associates
9217 Midwest Ave.
Cleveland, Ohio 44125

Technology for Energy Corporation
One Energy Center
Pellissippi Pkwy.
Knoxville, TN 37922
Attn: E. P. Stroupe

EG&G Idaho
Willow Creek Bldg. W-3
PO Box 1625
Idaho Falls, ID 83415
Attn: B. Barnes, T. L. Bridges,
J. A. Hunter (3 copies)

EG&G
Energy Measurements Group
Kirtland Operations
P. O. Box 4339, Station A
Albuquerque, NM 87196
Attn: W. Chaney

Sargent & Lundy Engineers
55 E Monroe St.
Chicago, IL 60603
Attn: A. Walser

General Electric Company
175 Curtner Ave.
San Jose, CA 95125
Attn: J. E. Love, E. O. Swain,
D. K. Henrie (3 copies)

R. F. Reedy, Inc.
236 N Santa Cruz Ave.
Los Gatos, Ca 95030

US Department of Energy
Office of Nuclear Energy
Mail Stop B-107
NE-540
Washington, DC 20545
Attn: A. Millunzi

Quadrex Corporation
1700 Dell Ave.
Campbell, CA 95008
Attn: Quazi A. Hossain

Chiapetta, Welch & Associates. Ltd.
9748 Roberts Rd.
Palos Hills, IL 60465
Attn: R. L. Chiapetta

ANATECH International Corp.
3344 N. Torrey Pines Court
Suite 320
LaJolla, CA 92037
Attn: Y. R. Rashid

Dr. Steve Hodge
Union Carbide Corp.
Building 9108
PO Box Y
Oak Ridge, TN 37830

Dr. Trever Pratt
Building 130
Brookhaven National Laboratory
Upton, NY 11973

Dr. Joseph J. Ucciferro
Structural Analysis Group
United Engineers & Constructors, Inc.
30 S 17th St.
Philadelphia, PA 19101

Electrical Power Research Institute
3412 Hillview Avenue, PO Box 10412
Palo Alto, CA 94304
Attn: Dr. H. T. Tang, Dr. Y. K. Tang
Dr. Ian Wall, Dr. Raf Sehgal
J. J. Taylor (5 copies)

Commissariat a L'Energie Atomique (CEA)
Centre d'Etudes Nucleaires de Saclay
F-91191 Gif-Sur-Yyette Cedex
France
Attn: M. Livolant, P. Jamet (2 copies)

Professor Richard N. White
School of Civil & Environ. Engr.
Hollister Hall Cornell University
Ithaca, NY 14853

Motor-COLUMBUS Consulting Engineers, Inc.
Parkstrasse 27
CH-5401 Baden
Switzerland
Attn: K. Gahler, J. Jemielewski
A. Schopfer (3 copies)

University of Tokyo
Institute of Industrial Science
22-1, Roppongi 7
Minatu-ku
Tokyo
Japan
Attn: H. Shibata

Argonne National Laboratory
9700 South Cass Avenue
Argonne, IL 60439
Attn: T. R. Bump, B. J. Hsieh,
M. H. Shackelford, S. H. Fistedis,
J. M. Kennedy, R. F. Kulak
R. W. Seidensticker,
G. A. McLennan (8 copies)

Dr. O. Mercier
EIR (Swiss Federal Institute for
Reactor Research)
CH-5303 Wuerlingen
Switzerland

Prof. Dr. H. Karwat
Lehrstuhl fuer Reakordynamik
und Reaktorsicherheit
Technische Universitaet Muenchen
D-8046 Garching
Federal Republic of Germany

Prof. Dr.-Ing. K. F. Kussmaul
Staatliche Materiapruefungsanstalt (MPA)
University of Stuttgart
Pfaffenwaldring 32
D-7000 Stuttgart 80
Federal Republic of Germany

Gesellschaft fuer Reaktorsicherheit (GRS)
Schwertnergasse 1
Federal Republic of Germany
Attn: H. Schulz, A. Hoefler (2 copies)

S. Chakraborty
Swiss Federal Nuclear Safety Inspectorate
Federal Office of Energy
CH-5303 Wuerenlingen
Switzerland

W. R. Conley
David Taylor Naval Ship R&D Center
Code 1750.2
Bethesda, Maryland 20084

Mr. Nathaniel Foster
Tennessee Valley Authority
400 Summit Hill Rd.
W9D24C-K
Knoxville, Tennessee 37902

1520 D. J. McCloskey
1523 R. C. Reuter
1523 C. Conley
1524 J. Jung
1833 G. A. Knorovsky
3141 C. M. Ostrander (5)
3151 W. L. Garner
6241 D. L. Goodwin
6400 A. W. Snyder
6410 J. W. Hickmann
6420 J. V. Walker
6440 D. A. Dahlgren
6442 W. A. von Riesemann (15)
6442 D. B. Clauss (5)
6442 D. S. Horschel
6442 L. N. Koenig
6442 D. L. Lambert
6442 P. E. Matson
6442 T. D. Molina
6444 L. D. Buxton
6446 L. L. Bonzon
6447 D. L. Berry
6449 K. D. Bergeron
7485 P. C. McKey
7485 F. H. Gallagos
7485 D. Leyva
7541 R. T. Reese
8024 M. A. Pound

NRC FORM 335 (2-84) NRCM 1102, 3201, 3202

U.S. NUCLEAR REGULATORY COMMISSION

BIBLIOGRAPHIC DATA SHEET

SEE INSTRUCTIONS ON THE REVERSE

1. REPORT NUMBER (Assigned by TIDC, add Vol. No., if any)
NUREG/CR-4209
SAND85-0679

2. TITLE AND SUBTITLE
Comparison of Analytical Predictions and Experimental Results for a 1:8-Scale Steel Containment Model Pressurized To Failure

3. LEAVE BLANK

4. DATE REPORT COMPLETED
MONTH: June
YEAR: 1985

5. AUTHOR(S)
David B. Clauss

6. DATE REPORT ISSUED
MONTH:
YEAR:

7. PERFORMING ORGANIZATION NAME AND MAILING ADDRESS (Include Zip Code)
Sandia National Laboratories
Containment Integrity Division
Albuquerque, NM 87185

8. PROJECT/TASK/WORK UNIT NUMBER

9. FIN OR GRANT NUMBER
NRC FIN NO. A1401

10. SPONSORING ORGANIZATION NAME AND MAILING ADDRESS (Include Zip Code)
Division of Engineering Technology
Office of Nuclear Regulatory Research
U.S. Nuclear Regulatory Commission
Washington, DC 20555

11a. TYPE OF REPORT
Topical

b. PERIOD COVERED (Inclusive dates)

12. SUPPLEMENTARY NOTES

13. ABSTRACT (200 words or less)

Predictions for the response of a 1:8-scale model of a steel nuclear containment building to overpressurization are compared to experimental results. Finite element analyses were used to predict the model's response. Strains, displacements, and leak rate measurements were made at 21 different pressure levels. Comparisons of the pressure histories for strain and displacement at a point, and the spatial variation of strain and displacement are made. In addition, comparisons of a more global nature, such as the capacity of the model and the failure mode, are discussed. An evaluation of the predictive capabilities and the failure criteria is made in the light of these comparisons.

14. DOCUMENT ANALYSIS - a. KEYWORDS/DESCRIPTORS

b. IDENTIFIERS/OPEN ENDED TERMS

15. AVAILABILITY STATEMENT
Unlimited

16. SECURITY CLASSIFICATION
(This page)
U
(This report)
U

17. NUMBER OF PAGES

18. PRICE

120555078877 1 1AN1R11RD
US NRC
ADM-DIV OF TIDC
POLICY & PUB MGT BR-PDR NUREG
W-501
WASHINGTON DC 20555